

6-1-2016

# Mg<sup>2+</sup> Differentially Regulates Two Modes of Mitochondrial Ca<sup>2+</sup> Uptake in Isolated Cardiac Mitochondria: Implications for Mitochondrial Ca<sup>2+</sup> Sequestration

Christoph A. Blomeyer  
*Medical College of Wisconsin*

Jason Bazil  
*University of Michigan - Ann Arbor*

David F. Stowe  
*Marquette University*

Ranjan K. Dash  
*Medical College of Wisconsin*

Amadou KS Camara  
*Medical College of Wisconsin*

---

Accepted version. *Journal of Bioenergetics and Biomembranes*, Vol. 48, No. 3 (June 2016): 175-188.

DOI. © 2016 Springer Science+Business Media. Used with permission.

The final publication is available at Springer via <http://dx.doi.org/10.1007/s10863-016-9644-1>.

David F. Stowe was also affiliated with the Medical College of Wisconsin and Zablocki Veterans Affairs Medical Center at the time of publication.

Ranjan K. Dash was also affiliated with the Medical College of Wisconsin at the time of publication.

Shareable Link. Provided by the Springer Nature [SharedIt](#) content-sharing initiative.

# Mg<sup>2+</sup> Differentially Regulates Two Modes of Mitochondrial Ca<sup>2+</sup> Uptake in Isolated Cardiac Mitochondria: Implications for Mitochondrial Ca<sup>2+</sup> Sequestration

C.A. Blomeyer

*Department of Anesthesiology, Medical College of Wisconsin  
Milwaukee, WI*

J.N. Bazil

*Department of Molecular and Integrative Physiology,  
University of Michigan,  
Ann Arbor, MI*

*Biotechnology and Bioengineering Center,  
Medical College of Wisconsin,  
Department of Physiology, Medical College of Wisconsin,  
Milwaukee, WI*

D.F. Stowe

*Department of Anesthesiology, Medical College of Wisconsin  
Department of Physiology, Medical College of Wisconsin  
Department of Biomedical Engineering, Marquette University  
Research Service, Zablocki Veterans Affairs Medical Center,  
Milwaukee, WI*

**R.K. Dash**

*Biotechnology and Bioengineering Center,  
Medical College of Wisconsin*

*Department of Physiology, Medical College of Wisconsin  
Department of Biomedical Engineering, Marquette University,  
Milwaukee, WI*

**A.K. Camara**

*Department of Anesthesiology, Medical College of Wisconsin,  
Milwaukee, WI*

**Abstract:** The manner in which mitochondria take up and store  $\text{Ca}^{2+}$  remains highly debated. Recent experimental and computational evidence has suggested the presence of at least two modes of  $\text{Ca}^{2+}$  uptake and a complex  $\text{Ca}^{2+}$  sequestration mechanism in mitochondria. But how  $\text{Mg}^{2+}$  regulates these different modes of  $\text{Ca}^{2+}$  uptake as well as mitochondrial  $\text{Ca}^{2+}$  sequestration is not known. In this study, we investigated two different ways by which mitochondria take up and sequester  $\text{Ca}^{2+}$  by using two different protocols. Isolated guinea pig cardiac mitochondria were exposed to varying concentrations of  $\text{CaCl}_2$  in the presence or absence of  $\text{MgCl}_2$ . In the first protocol, A,  $\text{CaCl}_2$  was added to the respiration buffer containing isolated mitochondria, whereas in the second protocol, B, mitochondria were added to the respiration buffer with  $\text{CaCl}_2$  already present. Protocol A resulted first in a fast transitory uptake followed by a slow gradual uptake. In contrast, protocol B only revealed a slow and gradual  $\text{Ca}^{2+}$  uptake, which was approximately 40 % of the slow uptake rate observed in protocol A. These two types of  $\text{Ca}^{2+}$  uptake modes were differentially modulated by extra-matrix  $\text{Mg}^{2+}$ . That is,  $\text{Mg}^{2+}$  markedly inhibited the slow mode of  $\text{Ca}^{2+}$  uptake in both protocols in a concentration-dependent manner, but not the fast mode of uptake exhibited in protocol A.  $\text{Mg}^{2+}$  also inhibited  $\text{Na}^+$ -dependent  $\text{Ca}^{2+}$  extrusion. The general  $\text{Ca}^{2+}$  binding properties of the mitochondrial  $\text{Ca}^{2+}$  sequestration system were reaffirmed and shown to be independent of the mode of  $\text{Ca}^{2+}$  uptake, i.e. through the fast or slow mode of uptake. In addition, extra-matrix  $\text{Mg}^{2+}$  hindered  $\text{Ca}^{2+}$  sequestration. Our results indicate that mitochondria exhibit different modes of  $\text{Ca}^{2+}$  uptake depending on the nature of exposure to extra-matrix  $\text{Ca}^{2+}$ , which are differentially sensitive to  $\text{Mg}^{2+}$ . The implications of these findings in cardiomyocytes are discussed.

**Keywords:** Mitochondria Cardiac Calcium uptake Calcium sequestration Calcium efflux

## Introduction

Mitochondria have the capacity to take up and sequester large amounts of  $\text{Ca}^{2+}$  (Vasington and Murphy 1962). For decades it was believed that mitochondrial  $\text{Ca}^{2+}$  was a necessary means to maintain proper energy balance in the heart. However, recent mitochondrial  $\text{Ca}^{2+}$  uniporter (MCU) knockout studies in mice have contested the importance of  $\text{Ca}^{2+}$  in mitochondrial energy homeostasis (Pan et al. 2013). Cardiac specific MCU knockout studies using a mouse model reveal that cardiac mitochondrial  $\text{Ca}^{2+}$  is only essential during high stress conditions, but not for routine activities (Kwong et al. 2015; Luongo et al. 2015; Wu et al. 2015). Whereas the role of mitochondria as a  $\text{Ca}^{2+}$  sink against cytosolic  $\text{Ca}^{2+}$  overload is well recognized (Szabadkai and Duchen 2008; Nicholls 2005; Rasola and Bernardi 2011), their role in shaping the cytosolic  $\text{Ca}^{2+}$  transients during physiological conditions is still debated (Boyman et al. 2014; Lu et al. 2013). Moreover, the precise mechanisms and consequences by which mitochondria take up, extrude, and sequester cytosolic  $\text{Ca}^{2+}$  remain obscure.

It has been suggested that mitochondrial  $\text{Ca}^{2+}$  uptake consists of different components that result in different matrix free  $\text{Ca}^{2+}$  dynamics. One possible component constitutes the rapid and beat-to-beat changes in the concentration of matrix free  $\text{Ca}^{2+}$  ( $[\text{Ca}^{2+}]_m$ ) (Dedkova and Blatter 2013; Huser et al. 2000). This fast mode of  $\text{Ca}^{2+}$  uptake is proposed to be responsible for regulating ATP production (Dedkova and Blatter 2013; Carafoli 2010; Tarasov et al. 2012) by altering activities of  $\text{Ca}^{2+}$ -sensitive dehydrogenases and other  $\text{Ca}^{2+}$ -sensitive processes. However, this idea, as noted above, is controversial based on recent data obtained from MCU knockout mice (Pan et al. 2013; Kwong et al. 2015). Another possible component that has been proposed is the slow mode of  $\text{Ca}^{2+}$  uptake, which functions as a low-pass filter of the cytosolic  $\text{Ca}^{2+}$  transient while gradually accumulating matrix  $\text{Ca}^{2+}$  (Dedkova and Blatter 2013; Sedova et al. 2006). It is also thought to be a significant source of  $\text{Ca}^{2+}$  uptake during periods of sustained elevation of cytosolic  $\text{Ca}^{2+}$  (Carafoli 2010; Dorn and Maack 2013), such as in ischemia and reperfusion (IR) injury (Varadarajan et al. 2001).

The MCU is the primary pathway for  $\text{Ca}^{2+}$  uptake (Baughman et al. 2011; De Stefani et al. 2011) and may possess multiple conductance modes (Kirichok et al. 2004; Wei et al. 2012; Csordas et al. 2013). The recent identities of the MCU channel and its regulatory proteins (e.g. MICU1 and MICU2) involved in modulating mitochondrial  $\text{Ca}^{2+}$  uptake are now characterized as sensors of extra-matrix  $[\text{Ca}^{2+}]$  ( $[\text{Ca}^{2+}]_e$ ) that stimulate or inhibit MCU, respectively. This would allow for a rapid response of mitochondria to  $\text{Ca}^{2+}$  signals generated in the cytoplasm (Marchi and Pinton 2014). Previous studies suggest that there exist additional potential  $\text{Ca}^{2+}$  uptake modes: the mitochondrial ryanodine-like receptor (Beutner et al. 2001; Tewari et al. 2014) and the rapid-mode (RaM) of  $\text{Ca}^{2+}$  uptake (Buntinas et al. 2001; Gunter et al. 1998; Sparagna et al. 1995). These fast modes of  $\text{Ca}^{2+}$  uptake were postulated, but not conclusively shown, to be responsible for transduction of physiological  $\text{Ca}^{2+}$  transients to match oxidative phosphorylation with energetic demands (Huser et al. 2000; O'Rourke and Blatter 2009).

Pharmacological inhibitors and/or modeling approaches have been used to identify the different modes of  $\text{Ca}^{2+}$  uptake, but the conclusions drawn from these studies have been disputed. For example, recent studies show relatively little mitochondrial  $\text{Ca}^{2+}$  uptake during physiological  $\text{Ca}^{2+}$  transients (Boyman et al. 2014; Lu et al. 2013), which implies that in the physiological setting, MCU might play only a negligible role in shaping physiological  $\text{Ca}^{2+}$  dynamics in the beating heart. Moreover, when mitochondria are loaded with sufficient  $\text{Ca}^{2+}$ , changes in matrix free  $\text{Ca}^{2+}$  are difficult to detect due to the higher buffering power associated with higher mitochondrial  $\text{Ca}^{2+}$  loads (Bazil et al. 2013; Blomeyer et al. 2013). Regardless, the MCU becomes most relevant when cytosolic  $[\text{Ca}^{2+}]$  is abnormally elevated, such as during IR, oxidative stress, sarcoplasmic reticulum stress, or  $\text{Ca}^{2+}$  overload (Varadarajan et al. 2001; An et al. 2001a; Rhodes et al. 2003; An et al. 2001b).

Excess  $\text{Ca}^{2+}$  uptake by mitochondria is sequestered in a phosphate-dependent reaction that forms amorphous calcium phosphate (CaPi) granules (Chalmers and Nicholls 2003; Greenawalt et al. 1964; Kristian et al. 2007). The exact composition of these CaPi granules is unknown, but they are presumed to consist of mixtures of  $\text{Ca}_3(\text{PO}_4)_2$ ,  $\text{Ca}_8\text{H}_2(\text{PO}_4)_6$ , and  $\text{Ca}_{10}(\text{PO}_4)_6(\text{OH})_2$  (Thomas and Greenawalt

1968). The properties of this sequestration system are a current area of interest because the buffering system alters both  $\text{Ca}^{2+}$  uptake and release dynamics (Blomeyer et al. 2013), and may regulate mitochondrial permeability transition (mPTP) (Szabadkai and Duchon 2008; Wei et al. 2012), which in turn may regulate mitochondrial  $\text{Ca}^{2+}$  transients (Sareen et al. 2007). In the heart and other excitatory tissues, the mitochondrial  $\text{Na}^+/\text{Ca}^{2+}$  exchanger (mNCE) is the primary pathway for  $\text{Ca}^{2+}$  extrusion (Boyman et al. 2013; Cai and Lytton 2004; Palty et al. 2004). Therefore,  $[\text{Ca}^{2+}]_m$  is primarily maintained by a balance of  $\text{Ca}^{2+}$  uptake facilitated by the MCU,  $\text{Ca}^{2+}$  extrusion by the mNCE, and  $\text{Ca}^{2+}$  buffering by the sequestration system. The sequestration system acts as a  $\text{Ca}^{2+}$  reservoir so that the activities of MCU and mNCE establish a set point that helps maintain sub-lethal thresholds of cytosolic  $\text{Ca}^{2+}$  during  $\text{Ca}^{2+}$  loading conditions.

Thus, the modes of mitochondrial  $\text{Ca}^{2+}$  uptake and their regulation remain obscure. Interestingly, in a recent study, we reported that mitochondrial  $\text{Ca}^{2+}$  uptake displays two different profiles of matrix  $\text{Ca}^{2+}$  transient when  $\text{CaCl}_2$  was added to mitochondrial suspension: a fast uptake of  $\text{Ca}^{2+}$  followed by a slower and more gradual uptake as matrix  $\text{Ca}^{2+}$  plateaus to a steady state (Boelens et al. 2013). Addition of  $\text{Mg}^{2+}$  to the respiration buffer appeared to have a differential effect on the two phases of the  $\text{Ca}^{2+}$  transient, with the slow phase attenuated more than the fast uptake phase. However, the impact of  $\text{Mg}^{2+}$  on mitochondria buffering of  $\text{Ca}^{2+}$  is not known. In the present study, we used a non-pharmacological approach to distinguish a slow and fast mode of mitochondrial  $\text{Ca}^{2+}$  uptake and determine the impact of extra-matrix  $\text{Mg}^{2+}$  on the modes of  $\text{Ca}^{2+}$  uptake and the mitochondrial buffering capacity or sequestration power of  $\text{Ca}^{2+}$ . To further delineate the two modes of  $\text{Ca}^{2+}$  uptake, mitochondria were exposed to two different protocols based on the order by which mitochondria or  $\text{CaCl}_2$  were first added to the respiration buffer with and without added  $\text{MgCl}_2$ .

## Methods

### *Mitochondrial isolation*

All experiments conformed to the Guide for the Care and Use of Laboratory Animals, and were approved by the Medical College of Wisconsin Institutional Animal Care and Use Committee. Mitochondria from guinea pig hearts were isolated as previously described (Blomeyer et al. 2013; Boelens et al. 2013; Aldakkak et al. 2013; Haumann et al. 2010). Briefly, guinea pigs (250–350 g) were anesthetized with intraperitoneal injection of 30 mg ketamine, and 700 units of heparin for anticoagulation. Hearts were excised and minced in ice-cold isolation buffer containing 200 mM mannitol, 50 mM sucrose, 5 mM  $\text{KH}_2\text{PO}_4$ , 5 mM MOPS, 1 mM EGTA and 0.1 % bovine serum albumin (BSA). Buffer pH was adjusted to 7.15 with KOH. The minced pieces were suspended in 2.65 ml ice-cold buffer with 5 U/ml protease (from *Bacillus licheniformis*) and homogenized at low speed for 30 s. Afterwards, 17 ml of ice-cold isolation buffer was added, and the suspension was again homogenized for 30 s and centrifuged at 8000 *g* for 10 min. The supernatant was discarded, and the pellet was re-suspended in 25 ml of ice-cold isolation buffer and centrifuged at 900 *g* for 10 min. The supernatant was recovered and centrifuged once more at 8000 *g* to yield the final mitochondrial pellet, which was re-suspended in isolation buffer and kept on ice (4 °C) for experiments after fluorescent dye loading to measure matrix  $\text{Ca}^{2+}$  transients.

The mitochondrial protein concentration was measured using the Bradford method (1976) and diluted with isolation buffer to a protein concentration of 5 mg/ml and incubated with the appropriate fluorescent dye or the vehicle (DMSO). Incubated mitochondria were re-suspended in 25 ml of ice-cold isolation buffer and re-centrifuged at 8000 *g*. Subsequently, the dye-loaded pellet was re-suspended in cold isolation buffer, and the protein concentration was measured again using the Bradford method and diluted finally to 12.5 mg/ml. The final mitochondrial suspension was kept in packed ice (4 °C), and all subsequent experiments were conducted within 6 h after the last step of the isolation procedure.

## *Experimental groups and protocols*

Isolated mitochondria were exposed to five different concentrations of CaCl<sub>2</sub> and three different concentrations of MgCl<sub>2</sub>. In addition, each of these groups was exposed to two different Ca<sup>2+</sup> loading protocols, resulting in 30 groups overall. The only difference between the two experimental protocols (A and B) was the order of addition of mitochondria and CaCl<sub>2</sub> to the respiration buffer containing pyruvic acid. Extra-matrix (buffer) free Ca<sup>2+</sup> ([Ca<sup>2+</sup>]<sub>e</sub>) and matrix free Ca<sup>2+</sup> ([Ca<sup>2+</sup>]<sub>m</sub>) were monitored under identical experimental conditions for both protocols, except for the order of addition of CaCl<sub>2</sub> or mitochondria to the buffer. For the NADH and ΔΨ<sub>m</sub> measurements, the number of experimental groups was reduced to eight for each experimental protocol (A and B). Each experiment was conducted with mitochondria pooled from 2 hearts and repeated 3–4 times on different days. Respiration buffer, which was adjusted to pH 7.15 with KOH, contained 130 mM KCl, 5 mM K<sub>2</sub>HPO<sub>4</sub>, 20 mM MOPS, 0.1 % BSA, and 40 μM EGTA (Blomeyer et al. 2013; Haumann et al. 2010). The mitochondrial concentration for all experiments was 0.5 mg/mL. The pH of the respiratory buffer remains at 7.15 after the addition of CaCl<sub>2</sub> and other substances, which was verified using a self-calibrating pH meter at the end of each experiment.

All experiments were conducted at room temperature (25 °C) using the cuvette-based fluorescence spectrophotometer described in our previous studies (Blomeyer et al. 2013; Boelens et al. 2013; Haumann et al. 2010; Agarwal et al. 2012, 2014; Aldakkak et al. 2011). Pyruvic acid (PA, 0.5 mM), cyclosporine A (CsA, 0.5 μM) and MgCl<sub>2</sub> (0, 0.5, 1.0 mM) were always present in the buffer. Ruthenium red (RR, 1 μM) was added at 300 s after all of the Ca<sup>2+</sup> bolus was taken up. The volume of the experimental buffer in the cuvette containing no added EGTA, and before adding any substance was 910 μL. The volume of added substances (PA, MgCl<sub>2</sub>, CaCl<sub>2</sub>, CsA, NaCl) to the cuvette was 10 μL each and the volume of the mitochondrial suspension added to the cuvette was 40 μL resulting in a total volume of 1000 μl for each experiment in protocols A and B. At a final volume of 1000 μL, the dilution factor after the addition of mitochondria was 25 times. Since the initial concentration of mitochondria following isolation was 12.5 mg/mL, the final mitochondrial suspension was



0.5 mg/mL in each experiment. The addition of a 40  $\mu$ L volume of mitochondrial suspension, which had a concentration of 1 mM EGTA from the original mitochondrial suspension (12.5 mg/mL), resulted in a final EGTA concentration of approximately 40  $\mu$ M for the mitochondrial suspension in the cuvette. The experimental buffer had a  $[\text{Ca}^{2+}]_e$  of approximately 50 nM that was similar to  $[\text{Ca}^{2+}]_m$  before adding any  $\text{CaCl}_2$ .

The protocols (A and B) used to assess differences in  $[\text{Ca}^{2+}]$  dynamics are shown in Fig.1. In protocol A at  $t = 30$  s, 40  $\mu$ L mitochondrial suspension was added to the experimental buffer. At  $t = 60$  s, 0, 10, 20, 30 or 40  $\mu$ M total  $\text{CaCl}_2$  (10  $\mu$ L of concentrated solution) was added to the mitochondrial suspension. In protocol B at  $t = 30$  s, 0, 10, 20, 30 or 40  $\mu$ M total  $\text{CaCl}_2$  (10  $\mu$ L of concentrated solution) was added first to the experimental buffer followed by addition of 40  $\mu$ L mitochondrial suspension at  $t = 60$  s. A high-speed magnetic stirring bar was turned on at the onset of each experiment to ensure prompt and rapid continuous mixing of the cuvette contents. With this approach, the effect of high initial localized boluses of  $[\text{CaCl}_2]$  on mitochondria in protocol A was minimized. In both protocols at  $t = 300$  s, 1  $\mu$ M RR was added to block the MCU and to prevent  $\text{Ca}^{2+}$  re-uptake after its release via the NCE. At  $t = 360$  s, 10 mM NaCl was added to induce  $\text{Ca}^{2+}$  efflux. The respiration buffer including the added PA was  $\text{Na}^+$ -free, except for the NaCl added at the end of each protocol to elicit  $\text{Ca}^{2+}$  release via mNCE activation. To avoid differences in buffer volume, the vehicle (de-ionized  $\text{H}_2\text{O}$ ) was used for 0 mM  $\text{MgCl}_2$  and 0  $\mu$ M  $\text{CaCl}_2$ . Some additional experiments (not shown) were conducted in the presence of the mNCE inhibitor, CGP-37,157 (25  $\mu$ M; Tocris Bioscience, Minneapolis, MN), to verify that the observed  $\text{Na}^+$ -induced  $\text{Ca}^{2+}$  efflux was due only to mNCE activity. All chemicals were obtained from Sigma-Aldrich (St. Louis, MO) unless noted otherwise.

### *Assessment of mitochondrial functional integrity*

Before and after fluorescence measurements were made using the PTI spectrofluorometer, mitochondrial functional integrity/viability was assessed by measuring the respiratory control index (RCI) with a Clark type  $\text{O}_2$  electrode (MT200A, Strathkelvin Instruments, Glasgow, UK). The RCI of mitochondria energized with 0.5 mM PA was

calculated by dividing the rate of state 3 respiration (250  $\mu\text{M}$  ADP) by the rate of state 4 respiration. Before the start of fluorescent measurements, RCI values were above 12 and at the end of the measurements (after approximately 6 h) RCI values were reevaluated and remained above 8. This strong RCI after 6 h indicates that the mitochondria were viable and well coupled for the duration of the experiments.

## *Fluorescence measurements*

Fluorescence spectrophotometry (Qm-8, Photon Technology International, Birmingham, NJ) was used to assess levels of  $[\text{Ca}^{2+}]_e$  and  $[\text{Ca}^{2+}]_m$ ,  $\Delta\Psi_m$ , and NADH. Fura-4F (Invitrogen™, Eugene, OR) was used to measure either  $[\text{Ca}^{2+}]_m$  (AM form) or  $[\text{Ca}^{2+}]_e$  (penta-potassium salt). For  $[\text{Ca}^{2+}]_m$  measurements, mitochondria were incubated for 30 min at room temperature (25 °C) with Fura-4F AM (5  $\mu\text{M}$ ) dissolved in DMSO. A final spin and resuspension of mitochondria were performed to remove any residual dye. To measure  $[\text{Ca}^{2+}]_e$ , Fura-4F penta-potassium (1  $\mu\text{M}$ ) was added to the respiration buffer.  $\Delta\Psi_m$  was measured using the lipophilic dye TMRM (1  $\mu\text{M}$ , Invitrogen™, Eugene, OR) in a ratiometric excitation approach (Scaduto and Grotyohann 1999). NADH was measured by its autofluorescence (Blomeyer et al. 2013; Boelens et al. 2013; Haumann et al. 2010). To ensure identical conditions as for the  $[\text{Ca}^{2+}]_m$  measurement, mitochondria were incubated with the appropriate concentration of DMSO for 30 min at 25 °C before measuring  $[\text{Ca}^{2+}]_e$ ,  $\Delta\Psi_m$ , and NADH.  $[\text{Ca}^{2+}]_e$  and  $\Delta\Psi_m$  were measured by directly adding the appropriate dye to the respiration buffer.

## *Measurement of free $\text{Ca}^{2+}$*

The  $\text{Ca}^{2+}$  measurements in this study represent the free matrix and extra-matrix  $\text{Ca}^{2+}$  for both protocols whereas the added  $\text{CaCl}_2$  (10–40  $\mu\text{M}$ ) represents the total amount of  $\text{CaCl}_2$  added to the cuvette. The molecular dye Fura-4F was used to measure concentrations of both matrix and extra-matrix free  $\text{Ca}^{2+}$ . The vendor specified dissociation constant ( $K_d$ ) of Fura-4F is 770 nM. However, when loaded in mitochondria, we determined a  $K_d$  of 890 nM. At an emission wavelength ( $\lambda_{em}$ ) of 510 nm, the peak of the excitation wavelength

( $\lambda_{ex}$ ) of Fura-4F shifted from 380 nm to 340 nm on binding  $Ca^{2+}$  to the dye molecules. Measuring  $Ca^{2+}$  at these wavelengths was not influenced by background noise (e.g. NADH autofluorescence), so a background subtraction was unnecessary. For calibration, ratios were obtained when all Fura-4F had become bound to  $Ca^{2+}$  ( $R_{max}$ ) and when no  $Ca^{2+}$  was bound to Fura-4F ( $R_{min}$ ). To determine these ratios, experiments were conducted in PA energized mitochondria using 500 nM CsA, 500  $\mu$ M  $CaCl_2$  for  $R_{max}$ , and A23187 ( $Ca^{2+}$ -ionophore) in the presence of 2.5 mM EGTA for  $R_{min}$ . The  $[Ca^{2+}]_m$  was calculated using the following equation (Grynkiewicz et al. 1985):

$$[Ca^{2+}]_m = K_d \cdot \frac{S_{f2}}{S_{b2}} \cdot \frac{R - R_{min}}{R_{max} - R} \quad (1)$$

$K_d$  is 890 nM,  $S_{f2}$  is the signal intensity of free Fura-4F measured at 380 nm, and  $S_{b2}$  is the signal intensity of  $Ca^{2+}$ -saturated Fura-4F measured at 380 nm. Their values were obtained from the  $R_{max}$  and  $R_{min}$  experiments, which were done for each preparation. For details, see Supplemental Figs. S1 and S2 for the fluorescence spectra in the presence of various amounts of  $Ca^{2+}$  and calibration of Fura-4F, respectively. Calibration of the Fura-4F penta-potassium signal in the presence of mitochondria was slightly different from the one used for Fura-4F AM.  $R_{min}$  was measured in respiration buffer with added 100  $\mu$ M EGTA without added  $CaCl_2$  to chelate all the  $Ca^{2+}$ , while  $R_{max}$  was determined in the respiration buffer containing 1 mM  $CaCl_2$ .  $Ca^{2+}$  fluorescent measurements and calculation of  $[Ca^{2+}]_e$  were conducted in the same manner as described above for  $[Ca^{2+}]_m$ . Free  $[Mg^{2+}]$  was not measured in this study. Our previous study showed that the calculated buffer  $[Mg^{2+}]$  after adding  $MgCl_2$  was nearly identical to the  $[Mg^{2+}]$  measured using Mag-Fura-2 fluorescence (Boelens et al. 2013).

## Measurement of NADH

NADH autofluorescence signals were measured at  $\lambda_{ex}$  of 350 nm and  $\lambda_{em}$  of 456 nm. For calibration, the NADH pool was either fully oxidized (0 %) with the respiratory uncoupler carbonyl cyanide 3-chlorophenylhydrazone (CCCP, 4  $\mu$ M), or fully reduced (100 %) with the complex I blocker rotenone (10  $\mu$ M).

## *Measurement of $\Delta\Psi_m$*

Fluorescence changes using TMRM were detected by two  $\lambda_{\text{ex}}$  (546 and 573 nm) and one  $\lambda_{\text{em}}$  (590 nm). Using the ratio of the emission at both excitation wavelengths (573/546) has the advantage of a higher dynamic range when compared to a single wavelength technique (Scaduto and Grotyohann 1999). At the end of each protocol at  $t = 720$  s, CCCP (4  $\mu\text{M}$ ) was added to fully depolarize mitochondria.

## *Statistical analyses*

The data from four hearts were pooled separately for each of the four fluorescence measurements. Data were transferred from PTI FelixGX (Version 3) into Microsoft® Excel® (2007). IBM® SPSS® (Version 19) was used to execute statistical analysis, which was performed using one-way analysis of variance followed by post hoc Tukey's range test to examine differences among individual groups. Changes were considered statistically significant when the  $p$ -value was set at  $\leq 0.05$ . Data for analyses were collected at the times given below and are presented as means  $\pm$  SEM. For some analyses, results are presented as means  $\pm$  standard deviation. Statistical tests were performed to compare changes in  $[\text{Ca}^{2+}]_m$  averaged from 60 to 70 s of all 30 possible treatment combinations for the five  $[\text{CaCl}_2]$ , three  $[\text{MgCl}_2]$ , and two protocol effects.

## *Calculation of mitochondrial $\text{Ca}^{2+}$ buffering power*

Initial rates of  $\text{Ca}^{2+}$  flux for both the uptake and extrusion phases were derived from the data and converted from  $d[\text{Ca}^{2+}]_e/dt$  to  $d[\text{Ca}^{2+}]_{\text{tot}}/dt$  using the method outlined in Bazil et al. (2013). Briefly, non-linear trend lines were fitted to the data shown in Figs. 2 and 4, and the analytical derivatives were used to compute the rate of change in free  $\text{Ca}^{2+}$ . Trend line fits to the extra-matrix and matrix dynamics are shown in Supplemental Figs. S4 and S5, respectively. The extra-matrix rates were converted to total  $\text{Ca}^{2+}$  flux by using the known buffering power of EGTA. For simplicity, all  $\text{Ca}^{2+}$  uptake rates were assumed to be through the MCU and all  $\text{Ca}^{2+}$  release rates were assumed to be via the NCE. To compute the mitochondrial  $\text{Ca}^{2+}$  buffering power, the approach described in Bazil et al. (2013) was

used. Specifically, the buffering power was calculated using the  $\text{Ca}^{2+}$  extrusion phase of the free  $\text{Ca}^{2+}$  dynamics profiles. The calculated  $\text{Ca}^{2+}$  buffering power was expressed as:

$$\beta_{\text{Ca},m} = 1 + \sum_i \frac{n_i^2 [\text{Ca}^{2+}]_m^{n_i-1} [B_{\text{Ca},i}]_m}{K_{\text{Ca},i}^{n_i} (1 + [\text{Ca}^{2+}]_m / K_{\text{Ca},i}^{n_i})^2} \quad (2)$$

## Results

### *Changes in extra-matrix ionized $\text{Ca}^{2+}$*

The dynamics of extra-matrix free  $\text{Ca}^{2+}$  for each protocol (A and B) and experimental conditions are shown in Fig. 2. Fluorescence ratios were converted to concentrations using Eq. 1. Each panel consists of five different traces representing one concentration of  $\text{CaCl}_2$  added (0, 10, 20, 30, or 40  $\mu\text{M}$ ) at one of three fixed  $\text{MgCl}_2$  concentrations (0, 0.5, or 1.0 mM) in the presence of 40  $\mu\text{M}$  EGTA. The dynamics of lower  $\text{CaCl}_2$  concentrations (0, 10, and 20  $\mu\text{M}$ ) are illustrated in more detail in the insets that show axes with the same labels seen in the main figure panels. Panels a-c show the  $\text{Ca}^{2+}$  dynamics profile using Protocol A, whereas panels d-f depict the  $\text{Ca}^{2+}$  dynamics profile using protocol B.

On a gross scale, the rates of decrease in  $[\text{Ca}^{2+}]_e$  ( $\text{Ca}^{2+}$  uptake rates), magnitude of uptake before addition of RR, and the rates of increase in  $[\text{Ca}^{2+}]_e$  ( $\text{Ca}^{2+}$  efflux rates) after addition of NaCl, were similar in each protocol for the same  $[\text{CaCl}_2]$  and  $[\text{MgCl}_2]$  combination (Fig. 2). And as expected,  $\text{Ca}^{2+}$  uptake was attenuated when  $\text{MgCl}_2$  was included in the buffer. However, distinct differences in the rates of  $\text{Ca}^{2+}$  uptake between each protocol were revealed by careful analysis. Double exponential functions fit to the  $\text{Ca}^{2+}$  uptake dynamics for protocol A revealed that the overall dynamics consisted of two time scales as shown in Fig. 3. These trend lines were fit between 60 and 150 s of the early phase of the uptake as shown in Supplemental Fig. S4. A single exponential function was sufficient to characterize the  $\text{Ca}^{2+}$  uptake dynamics for protocol B for all  $[\text{CaCl}_2]$  and  $[\text{MgCl}_2]$  combinations except for 40  $\mu\text{M}$   $\text{CaCl}_2$  (data not shown). For this

concentration of  $\text{CaCl}_2$ , a double exponential function was a better fit with similar time constants for the 40  $\mu\text{M}$   $\text{CaCl}_2$  condition in protocol A. For additions of  $\text{CaCl}_2$  of 10  $\mu\text{M}$  and below, the dynamics of  $[\text{Ca}^{2+}]_e$  were at or below detectable limits and were not used in the analysis. Furthermore, adding 40  $\mu\text{M}$   $\text{CaCl}_2$  in the presence of 0.5 or 1.0 mM  $\text{MgCl}_2$  in either protocol induced a faster  $\text{Ca}^{2+}$  uptake rate compared to 30  $\mu\text{M}$   $\text{CaCl}_2$ , which resulted in lower levels of  $[\text{Ca}^{2+}]_e$  before addition of RR and NaCl.

### *Changes in matrix ionized $\text{Ca}^{2+}$*

Using the same protocols (A and B) shown in Fig. 1,  $\text{CaCl}_2$  was added and  $[\text{Ca}^{2+}]_m$  was measured. As with the extra-matrix  $\text{Ca}^{2+}$ , the fluorescent ratios were converted to concentrations using Eq. 1. Fura-4F AM loading and washout was confirmed by ensuring that  $[\text{Ca}^{2+}]_m$  did not change after adding EGTA to the buffer (not shown). The results are displayed in Fig. 4 with a similar layout of the figure panels (a–f) shown in Fig. 2. Note that a very high  $[\text{Ca}^{2+}]_m$  was attained because CsA had been added to the buffer in all experiments. Panels a–c and d–f show  $[\text{Ca}^{2+}]_m$  dynamics at 0, 0.5 and 1.0 mM  $\text{MgCl}_2$  using protocol A and protocol B, respectively. Matrix free  $\text{Ca}^{2+}$  dynamics were quantitatively and qualitatively different for each protocol and  $\text{CaCl}_2/\text{MgCl}_2$  combination. For protocol A (Fig. 4, panels a–c), adding  $\text{CaCl}_2$  (10, 20, 30, or 40  $\mu\text{M}$ ) induced an abrupt and rapid uptake of  $\text{Ca}^{2+}$ . Adding lower  $[\text{CaCl}_2]$  (10 and 20  $\mu\text{M}$ , see insets) caused smaller increases in peak  $[\text{Ca}^{2+}]_m$  compared to the higher  $[\text{CaCl}_2]$  (30 and 40  $\mu\text{M}$ ). Nonetheless, even at lower  $[\text{CaCl}_2]$  (10 and 20  $\mu\text{M}$ ), there was an abrupt increase in  $\text{Ca}^{2+}$  uptake when  $\text{CaCl}_2$  was added to mitochondria. Note that in protocol A the  $\text{Ca}^{2+}$  uptake at any  $[\text{CaCl}_2]$  showed an initial fast  $\text{Ca}^{2+}$  uptake phase followed by a slower gradual  $\text{Ca}^{2+}$  uptake phase. This fast uptake was not observed in protocol B.

Figure 5 shows the measured  $[\text{Ca}^{2+}]_m$  recorded over a few seconds (averaged from 60 to 70 s) for protocols A and B. For the 20 and 30  $\mu\text{M}$   $\text{CaCl}_2$  additions across all  $\text{MgCl}_2$  conditions using protocol A, there were statistically significant differences in  $[\text{Ca}^{2+}]_m$  when compared to the same  $\text{CaCl}_2$  and  $\text{MgCl}_2$  combination using protocol B ( $p \leq 0.05$ ). The presence of added  $\text{MgCl}_2$  in the respiration buffer attenuated the maximal  $[\text{Ca}^{2+}]_m$  in a concentration-dependent manner

at each  $[\text{CaCl}_2]$  except for the 40  $\mu\text{M}$   $\text{CaCl}_2$ . For protocol B (Fig. 4, panels d-f), mitochondrial  $\text{Ca}^{2+}$  uptake was slower and more gradual at the lower  $[\text{CaCl}_2]$  (10, 20, and 30  $\mu\text{M}$ ) as shown in the insets of Figs. 2 and 4. However, in the 40  $\mu\text{M}$   $\text{CaCl}_2$  group, adding mitochondria to respiration buffer with  $\text{CaCl}_2$  already present (protocol B) showed a similar fast  $\text{Ca}^{2+}$  uptake rate as observed in protocol A. After adding 40  $\mu\text{M}$   $\text{CaCl}_2$  in protocol B, the fluorescent signal was close to  $R_{\text{max}}$ ; thus the calculated  $[\text{Ca}^{2+}]_m$  was very noisy and likely not representative of the true value of  $[\text{Ca}^{2+}]_m$ . For protocol A and during exposure to low  $\text{CaCl}_2$  (10–30  $\mu\text{M}$ ), the  $[\text{Ca}^{2+}]_m$  attained during the slow uptake, but not the initial fast uptake phase, was significantly different among the  $\text{MgCl}_2$  additions for a given  $[\text{CaCl}_2]$ . Overall, a comparison of these protocols shows that there exists a  $\text{Mg}^{2+}$ -insensitive, fast component of  $\text{Ca}^{2+}$  uptake that appears only when  $\text{CaCl}_2$  is added to buffer already containing mitochondria, or when the  $[\text{CaCl}_2]$  is high enough. The addition of RR (1  $\mu\text{M}$ ) completely inhibited  $\text{Ca}^{2+}$  uptake in both protocols A and B. Furthermore, at 40  $\mu\text{M}$   $\text{CaCl}_2$  the similarity in the rate of uptake between the two protocols is a verification to the equivalent rapidity of mixing of substances added to the cuvette.

### *Changes in $\Delta\Psi_m$ and NADH*

In parallel studies,  $\Delta\Psi_m$  and NADH were measured to confirm that the differences observed in  $\text{Ca}^{2+}$  uptake dynamics were not due to changes in bioenergetics. Experimental conditions were simplified to consist of 0 and 1.0 mM  $\text{MgCl}_2$  and 0 and 40  $\mu\text{M}$   $\text{CaCl}_2$  combinations. Figure 6, panels a and b, and panels c and d, summarize changes in  $\Delta\Psi_m$  and NADH, respectively during protocol A and protocol B. Note that the starting point for the two variables in the figure were slightly different, with the start point at 30 and 60 s for protocols A and B, respectively. There were no significant differences observed in either  $\Delta\Psi_m$  or NADH between the two protocols. In addition,  $\Delta\Psi_m$  and NADH were not significantly affected by adding 40  $\mu\text{M}$   $\text{CaCl}_2$  (protocol A and B) in either the presence or absence of 1 mM  $\text{MgCl}_2$ , which indicates that mitochondrial bioenergetics was not affected by the nature of mitochondrial exposure to  $\text{CaCl}_2$  (protocol A vs. protocol B) or  $\text{MgCl}_2$ .

## *Mitochondrial Ca<sup>2+</sup> buffering power*

The Ca<sup>2+</sup> uptake dynamics obtained under protocols A and B that are shown in Figs. 2 and 4 were used to calculate the mitochondrial Ca<sup>2+</sup> buffering power ( $\beta_{Ca^{2+}_m}$ ) as a function of  $[Ca^{2+}]_m$  using Eq. 2 and shown in Fig. 7. At low  $[Ca^{2+}]_m$ ,  $\beta_{Ca^{2+}_m}$  was nearly 3000:1 (total matrix  $[Ca^{2+}]$ :free matrix  $[Ca^{2+}]$ ) but rose to 10,000:1 as  $[Ca^{2+}]_m$  was increased beyond 5  $\mu$ M. The calculated  $\beta_{Ca^{2+}_m}$  values for  $[Ca^{2+}]_m$  below 500 nM were highly variable due to the  $[Ca^{2+}]_m$  measurement limitations discussed above. When MgCl<sub>2</sub> was present,  $\beta_{Ca^{2+}_m}$  no longer increased as much and began to decrease as  $[Ca^{2+}]_m$  increased further in a concentration-dependent manner. Based on a two component-buffering model for matrix Ca<sup>2+</sup>, this decrease in  $\beta_{Ca^{2+}_m}$  is likely due to an effect of Mg<sup>2+</sup> to reduce the Ca<sup>2+</sup> binding capacity for the class 2 buffers. The effect of  $[Mg^{2+}]_e$  on the sequestration parameters is summarized in Table 1. Although higher  $[Ca^{2+}]_m$  were attained with protocol A due to increased MCU activity triggered by the activation of both fast and slow modes of Ca<sup>2+</sup> uptake,  $\beta_{Ca^{2+}_m}$  was invariant with respect to either protocol A or B and was uniquely set both by  $[Ca^{2+}]_m$  and by  $[Mg^{2+}]_e$ .

## *Mg<sup>2+</sup> attenuates both Ca<sup>2+</sup> uptake and efflux*

The data shown in Figs. 2 and 4 were also used to calculate the rates for the slow mode Ca<sup>2+</sup> uptake by MCU and extrusion by mNCE under the experimental conditions used in this study. Note that these transport rates were calculated using  $J_{Ca^{2+},tot} = (d[Ca^{2+}]_m/dt) * \beta_{Ca^{2+},m}$  within 10 s of CaCl<sub>2</sub> or NaCl-induced perturbations. Mg<sup>2+</sup> was found to attenuate both the slow mode of Ca<sup>2+</sup> uptake by MCU (Fig. 8a) and the release by mNCE (Fig. 8b). The slow mode Ca<sup>2+</sup> uptake rates in protocol B were about 40 % of the slow mode Ca<sup>2+</sup> uptake rates in protocol A for all three extra-matrix MgCl<sub>2</sub> levels. The extrusion rates were independent of the Ca<sup>2+</sup> loading protocol, i.e. protocol A vs. protocol B. These rates were estimated from the  $[Ca^{2+}]_e$  dynamics by averaging the rates between 75 and 90 s and 360–390 s for Ca<sup>2+</sup> uptake and extrusion, respectively.



## Discussion

### *Mitochondrial Ca<sup>2+</sup> uptake modes*

In our examination of factors that affect mitochondrial Ca<sup>2+</sup> handling (influx, efflux and sequestration), we measured extra-matrix and matrix free Ca<sup>2+</sup> dynamics in isolated cardiac mitochondria using various combinations of [CaCl<sub>2</sub>] and [MgCl<sub>2</sub>] under two different Ca<sup>2+</sup> loading protocols (Fig. 1). The order of addition, i.e. mitochondria before CaCl<sub>2</sub> or mitochondria after CaCl<sub>2</sub>, resulted in significant differences in mitochondrial Ca<sup>2+</sup> uptake dynamics. In protocol A, mitochondria displayed a fast Ca<sup>2+</sup> uptake profile at each [CaCl<sub>2</sub>] that was followed by a slower and more gradual Ca<sup>2+</sup> uptake profile when CaCl<sub>2</sub> was added first as a bolus and mitochondria after that in the presence or absence of MgCl<sub>2</sub>. These two modes are evident from the time constant analyses summarized in Fig. 3 and the degree of Ca<sup>2+</sup> uptake depicted in Fig. 5. In protocol B, when mitochondria were exposed to the buffer containing CaCl<sub>2</sub> already present with or without MgCl<sub>2</sub>, Ca<sup>2+</sup> uptake was slower and more gradual at CaCl<sub>2</sub> concentrations below 40 μM. Therefore, when compared to protocol A, only the slower mode of Ca<sup>2+</sup> uptake was apparent at the lower [CaCl<sub>2</sub>] in protocol B. These differences in Ca<sup>2+</sup> uptake between the two protocols were not due to differences in ΔΨ<sub>m</sub> as indicated in Fig. 4a, b. This finding is further supported by the data of Supplemental Fig. S3, which shows that in the absence of PA before adding CaCl<sub>2</sub> first or mitochondria first, the different uptake modes remained evident as in the original two main protocols in which PA was present. The presence of extra-matrix MgCl<sub>2</sub> markedly attenuated the slow, but not the fast, component of Ca<sup>2+</sup> uptake and altered mitochondrial Ca<sup>2+</sup> buffering (sequestration) power (Figs. 7 and 8). This is also evident by the decreasing effect of Mg<sup>2+</sup> on the slow time constants shown in Fig. 3. Also, note that the fast time constants were relatively insensitive to Mg<sup>2+</sup>, which further supports the Mg<sup>2+</sup> independent nature of the fast uptake shown in Fig. 5. These two potential modes of Ca<sup>2+</sup> uptake are consistent with our recent computational modeling report on the dynamics of Ca<sup>2+</sup> uptake (Tewari et al. 2014). Interestingly, the analysis also revealed that the slow mode was inhibited in protocol B reaching only 40 % of the rate observed during protocol A regardless of [Mg<sup>2+</sup>]<sub>e</sub> as shown in Fig. 8a (compare dashed lines vs. solid lines).

We suggest that there are two distinct modes of  $\text{Ca}^{2+}$  uptake that occur at physiological levels of cytosolic  $\text{Ca}^{2+}$  and  $\text{Mg}^{2+}$ . One mode is a fast,  $\text{Mg}^{2+}$ -insensitive  $\text{Ca}^{2+}$  uptake pathway that could be modeled as a RyR-type channel (Tewari et al. 2014) and the other is a slower  $\text{Mg}^{2+}$ -sensitive  $\text{Ca}^{2+}$  uptake pathway (Pradhan et al. 2011), that is also modulated by the mode of  $\text{Ca}^{2+}$  delivery. Moreover, the  $\text{Mg}^{2+}$ -insensitive nature of the fast mode we found in the present study is compatible with the data on  $\text{Mg}^{2+}$ -insensitive RaM of  $\text{Ca}^{2+}$  uptake reported by Gunter et al. (1998). Our findings are also consistent with the attenuating effect of  $\text{Mg}^{2+}$  on the slow mode of  $\text{Ca}^{2+}$  uptake reported earlier by our group (Boelens et al. 2013).

The focus of this study was not to characterize the regulatory action of the molecular components of the MCU complex; however, it suffices to note that the differences in uptake could be attributed to a differential regulation of MCU during exposure to different  $\text{CaCl}_2$  with and without  $\text{MgCl}_2$ . It is possible that the marked differences in the two modes of  $\text{Ca}^{2+}$  uptake we found are attributable to the MCU complex and its regulatory subunits, e.g. MICU1 and MICU2 (Marchi and Pinton 2014; Patron et al. 2014; Mallilankaraman et al. 2012). MICU1 appears to act in response to high cytosolic  $[\text{Ca}^{2+}]$  by stimulating  $\text{Ca}^{2+}$  uptake by MCU, whereas MICU2 appears to inhibit MCU functions at a lower cytosolic  $[\text{Ca}^{2+}]$  (Patron et al. 2014; Kamer and Mootha 2014). However, major controversies abound in these observations, with conflicting results reported (Marchi and Pinton 2014; Patron et al. 2014; Mallilankaraman et al. 2012). Some of the discrepancies might be due to the composition of the buffer. For example, in one report  $\text{Mg}^{2+}$ , an allosteric modulator of MCU activity was present, whereas in another study it was absent (Csordas et al. 2013; Mallilankaraman et al. 2012). And while incontrovertible evidence of MCU inhibition by  $\text{Mg}^{2+}$  exists (see, for example, Kirichok et al. 2004), the molecular components responsible remain unidentified. The ability of the  $\text{Ca}^{2+}$  delivery method to unmask different modes of MCU activity could be attributed to its effect on the state of the EF-hands located on the MICU1 and/or MICU2 regulatory subunits. For example, if the MICU1 and MICU2 subunits act in conjunction as a  $\text{Ca}^{2+}$ -sensitive break mechanism (Patron et al. 2014; Kamer and Mootha 2014), a rapid change in  $\text{Ca}^{2+}$  near the subunits may temporarily release the break and result in a brief, rapid uptake of  $\text{Ca}^{2+}$ . That said, the present study is focused on the observation of a fast and slow mode of  $\text{Ca}^{2+}$  uptake

that is dependent on the manner by which mitochondria are exposed to a bolus of  $\text{CaCl}_2$ , and not specifically on the regulation by MICU1, MICU2, and other regulatory proteins. Future elaborate studies in the contribution of these proteins to these two modes of  $\text{Ca}^{2+}$  in the presence and absence of  $\text{Mg}^{2+}$ , and the impact on the mitochondrial  $\text{Ca}^{2+}$  buffering capacity should be undertaken.

It is evident that mitochondria took up  $\text{Ca}^{2+}$  in a quick and robust manner when  $\text{CaCl}_2$  was added to the mitochondrial suspension (protocol A). In contrast, the matrix free  $\text{Ca}^{2+}$  dynamics data showed that when mitochondria were added to respiration buffer with  $\text{CaCl}_2$  already present, the fast uptake mode was abolished for all  $\text{CaCl}_2$  concentrations except for the highest [ $\text{CaCl}_2$ ] (40  $\mu\text{M}$ ). Note that the order of adding 40  $\mu\text{M}$   $\text{CaCl}_2$  and mitochondria to the respiration buffer resulted in similar  $\text{Ca}^{2+}$  uptake profile for both protocols. This indicates that the rapid mixing of the cuvette content assured near instantaneous homogenous mixture, and that the difference in  $\text{Ca}^{2+}$  uptake between the two protocols was mostly due to the different modes of uptake in mitochondria and not to an uneven mix of the added  $\text{CaCl}_2$ . The order of adding mitochondria or  $\text{CaCl}_2$  also did not affect the  $\Delta\Psi$  or redox state indicating that mitochondria were fully energized in the presence of PA when mitochondria were added before or after adding  $\text{CaCl}_2$ . These observations provide further evidence that the method of exposure to  $\text{Ca}^{2+}$ , and not bioenergetic differences such as  $\Delta\Psi$ , is the regulatory mechanism behind the vastly different uptake modes observed in our study. In addition, this difference in  $\text{Ca}^{2+}$  uptake was more apparent when  $\text{MgCl}_2$  was included in the respiration buffer of either  $\text{Ca}^{2+}$  loading protocol. This difference in the mode of  $\text{Ca}^{2+}$  uptake was also not dependent on the mitochondrial redox state because the NADH autofluorescence data (Fig. 6) showed no observable difference between the two protocols (A and B), in the presence or absence of added  $\text{CaCl}_2$  or  $\text{MgCl}_2$ .

Based on these observations, we can conclude that  $\text{Mg}^{2+}$  regulates bulk  $\text{Ca}^{2+}$  uptake by attenuating mainly the slow component of the MCU-mediated  $\text{Ca}^{2+}$  uptake in a concentration-dependent manner. This conclusion is supported by our previous findings (Boelens et al. 2013) and recent computational models (Tewari et al. 2014; Bazil and Dash 2011) and indicates that the MCU is capable of operating in multiple conductance modes. In addition, the data

revealed another intriguing aspect of the  $\text{Ca}^{2+}$ -dependent regulation of mitochondrial  $\text{Ca}^{2+}$  uptake. As shown in Fig. 2, the 40  $\mu\text{M}$   $\text{CaCl}_2$  bolus resulted in a lower  $[\text{Ca}^{2+}]_e$  at the time of RR addition compared to the 30  $\mu\text{M}$   $\text{CaCl}_2$  bolus for either protocol. In other words, a higher bolus of  $\text{CaCl}_2$  resulted in more  $\text{Ca}^{2+}$  being taken up by mitochondria, which was inhibited by  $\text{Mg}^{2+}$  in a concentration-dependent manner. We speculate that this phenomenon is due to differential regulation or modulation of MCU conductance/open probability times by other components of the protein complex (e.g. MICU1 and MICU2) (Kamer and Mootha 2014; Harrington and Murphy 2015).

The  $\text{Mg}^{2+}$ -sensitivity of the MCU complex likely plays a role in heart failure, ischemia and reperfusion injury, and other related events in the myocardium (for review see Douban et al. 1996; Kolte et al. 2014; Levitsky and Takahashi 2013). For example, cytosolic  $[\text{Mg}^{2+}]$  is known to rise during ischemia due to net ATP hydrolysis. This rise in  $[\text{Mg}^{2+}]$  would help mitigate mitochondrial  $\text{Ca}^{2+}$  loading via MCU, but the  $\text{Ca}^{2+}$  buffering system would be compromised, which could counter the  $\text{Mg}^{2+}$  effect and contribute to mitochondrial  $\text{Ca}^{2+}$  overload. In heart failure, the net decrease in cellular  $\text{Mg}^{2+}$  content would lead to more mitochondrial  $\text{Ca}^{2+}$  uptake via the MCU. Based on our results reported herein, the decrease in cytosolic  $[\text{Mg}^{2+}]$  levels observed in these pathophysiological conditions, e.g. heart failure, would likely result in elevated  $[\text{Ca}^{2+}]_m$ . This would likely induce  $\text{Ca}^{2+}$ -mediated mitochondrial dysfunction, and if the local cytosolic  $[\text{Ca}^{2+}]$  is high, also possibly trigger mPTP opening with concomitant cell death. Indeed, it has been reported that the cardiovascular consequences of  $\text{Mg}^{2+}$  deficiency in clinical studies include multifocal necrosis with  $\text{Ca}^{2+}$  accumulation in mitochondria in a pattern suggestive of myocardial infarction (Seelig 1989).

### *$\text{MgCl}_2$ and mitochondrial mNCE-induced $\text{Ca}^{2+}$ efflux*

The well-known effect of  $\text{Mg}^{2+}$  to attenuate  $\text{Ca}^{2+}$  uptake and its extrusion is demonstrated in greater detail by our data. The rate of increase in  $[\text{Ca}^{2+}]_m$  significantly decreased as a function of  $[\text{Mg}^{2+}]_e$  with an apparent  $K_i$  of 0.25 mM (Fig. 8a). This value is similar to that of our previously determined computational model of  $\text{Ca}^{2+}$  uptake (Pradhan et al. 2011). At 1 mM  $[\text{Mg}^{2+}]_e$ , close to the physiological extra-matrix

level, the MCU complex was inhibited by greater than 15-fold at the peak of a 1  $\mu\text{M}$  cytosolic  $\text{Ca}^{2+}$  transient. Despite this,  $[\text{Ca}^{2+}]_m$  reached close to 1  $\mu\text{M}$  with addition of 20  $\mu\text{M}$   $\text{CaCl}_2$  (Fig. 4c) due to the rapid uptake mode by the MCU complex. Incidentally,  $[\text{Mg}^{2+}]_e$  also inhibits  $\text{Na}^+$ -dependent  $\text{Ca}^{2+}$  efflux (Wingrove and Gunter 1986), which is consistent with some of our current findings (Fig. 8b). Here, it is shown that  $\text{Mg}^{2+}$  with a  $K_i$  of 1 mM inhibited the rate of decrease in  $[\text{Ca}^{2+}]_m$ . Moreover, the maximal rate of  $\text{Ca}^{2+}$  efflux was reduced to half when  $[\text{Mg}^{2+}]_e$  was increased from 0 mM to 1 mM. So not only is  $\text{Ca}^{2+}$  uptake slowed when there is an increase in  $[\text{Mg}^{2+}]_e$ , but also the rate of  $\text{Ca}^{2+}$  extrusion is impeded. Whereas it appears to be clear that  $[\text{Mg}^{2+}]_e$  regulates the slower phase of  $\text{Ca}^{2+}$  uptake, the  $\text{Mg}^{2+}$ -insensitive rapid component of the MCU complex can lead to net  $\text{Ca}^{2+}$  uptake when mitochondria are presented with sufficiently high, pulse-like  $\text{Ca}^{2+}$  transients.

### *Mitochondrial $\text{Ca}^{2+}$ buffering*

The data from this study also corroborates previous reports that the mitochondrial  $\text{Ca}^{2+}$  sequestration system consists of at least two classes of buffers (Wei et al. 2012; Bazil et al. 2013; Blomeyer et al. 2013) (Fig. 7) and challenges recent findings (Wei et al. 2012; Tewari et al. 2014) that suggest the manner in which  $\text{Ca}^{2+}$  is loaded into mitochondria (fast vs. slow) modulates the degree of  $\text{Ca}^{2+}$  buffering. In our prior study, we used indo-1 to monitor  $[\text{Ca}^{2+}]$  in both the extra-matrix and matrix compartments and mitochondrial  $\text{Ca}^{2+}$  buffering (Blomeyer et al. 2013). In contrast, in the current study we used Fura-4F because it can register higher  $[\text{Ca}^{2+}]$  than indo-1 without saturating. Consequently, we also added CsA to the experimental buffer to prevent mPTP opening induced by high  $[\text{Ca}^{2+}]_m$ . As a result of using a different  $\text{Ca}^{2+}$  indicator dye and different experimental conditions, we observed somewhat different buffering parameters between the current and previous studies (Bazil et al. 2013; Blomeyer et al. 2013) that can be explained by the different extent of dye loading, cation binding properties between each type of  $\text{Ca}^{2+}$  fluorescence dye, and experimental conditions. Despite these differences, the general properties of the sequestration system identified in this study are identical to our previous reports (Bazil et al. 2013; Blomeyer et al. 2013). That is, the class 1 buffers are of the

prototypical type and consist of binding sites that bind a single  $\text{Ca}^{2+}$  ion, whereas the class 2 buffers are capable of binding multiple  $\text{Ca}^{2+}$  ions at a single site in a cooperative fashion.

There is strong supporting evidence that the class 2 buffers consist of complexes formed by the annexin class of proteins in conjunction with acidic phospholipids in the membrane that promote or facilitate the formation of CaPi granules on the inner leaflets of the inner mitochondrial membrane (IMM) (for discussion, see Bazil et al. 2013). In our present study, we show that  $\text{Mg}^{2+}$  also modulates this class of  $\text{Ca}^{2+}$  buffers but does not regulate the class 1 buffers (Fig. 7). The mechanisms by which  $\text{Mg}^{2+}$  alters  $\text{Ca}^{2+}$  sequestration is unclear but may involve two mechanisms: i) extra-mitochondrial  $\text{Mg}^{2+}$  alters the class 2 buffer affinity for  $\text{Ca}^{2+}$  or ii) matrix  $\text{Mg}^{2+}$  encumbers the formation of CaPi complexes in the matrix on the surface of the IMM. We propose that latter is more likely. Based on earlier reports by Brierley et al. (1962, 1963, 1964),  $\text{Mg}^{2+}$  is actively loaded into energized mitochondria in a Pi-dependent and -independent manner. Therefore, Pi levels might modulate  $\text{Mg}^{2+}$  uptake during  $\text{Ca}^{2+}$  loading which would result in an increase in matrix  $\text{Mg}^{2+}$  content. However, Boelens et al. (2013) reported that increasing buffer  $\text{MgCl}_2$  did not change  $[\text{Mg}^{2+}]_m$  appreciably over time. In that study,  $\text{Ca}^{2+}$  uptake was absent, and the internal mechanisms regulating matrix  $\text{Mg}^{2+}$  were already in homeostasis. A plausible hypothesis is that  $\text{Mg}^{2+}$  enters mitochondria concomitantly with  $\text{Ca}^{2+}$  and interferes with CaPi granule formation. This is consistent with the observation that  $\text{Mg}^{2+}$  prevents and slows the spontaneous transition of CaPi from an amorphous state to a crystalline state (Wu et al. 2008, 2009). Nevertheless, our results demonstrate that when  $[\text{Mg}^{2+}]_e$  is elevated, the ability of mitochondria to sequester large amounts of  $\text{Ca}^{2+}$  is hindered.

### *Summary and perspective*

The mechanism by which isolated mitochondria take up and sequester  $\text{Ca}^{2+}$  is a complex function not only of how much  $\text{Ca}^{2+}$  mitochondria are exposed to, but also the experimental conditions. In one scenario, when added  $\text{CaCl}_2$  exceeds a threshold, a rapid,  $\text{Mg}^{2+}$ -insensitive mode of  $\text{Ca}^{2+}$  uptake is activated. In another scenario, when mitochondria are added to the buffer with low concentrations of

EGTA and CaCl<sub>2</sub> already present, the rapid mode of Ca<sup>2+</sup> uptake is not activated, that is unless the buffer concentration of CaCl<sub>2</sub> is sufficiently high. Thus, the MCU appears to consist of multiple conductance modes, which are differentially modulated by extra-matrix Mg<sup>2+</sup>.

Mitochondrial Ca<sup>2+</sup> homeostasis plays important roles in cellular physiology, regulation of cellular bioenergetics, reactive oxygen species signaling and Ca<sup>2+</sup> signaling. Agonist-induced intracellular Ca<sup>2+</sup> signals can be rapidly transduced to the matrix because mitochondria can exist in close apposition to sites of Ca<sup>2+</sup> release where local cytosolic [Ca<sup>2+</sup>] can be higher than in the rest of the cytoplasm (Mallilankaraman et al. 2012). The physiological implications of the different modes of Ca<sup>2+</sup> uptake in this study are unclear but allude to a process whereby mitochondria can rapidly accumulate and sequester Ca<sup>2+</sup> to prevent catastrophic cytosolic Ca<sup>2+</sup> overload, mPTP opening and cell death. Therefore, a better understanding of the Ca<sup>2+</sup> dynamics and how it is modulated by physiological [Mg<sup>2+</sup>] could provide new insights into the potential molecular mechanisms that regulate Ca<sup>2+</sup> fluxes in and out of mitochondria under both physiological and pathophysiological conditions.

## Acknowledgments

This work was funded by NIH grants R01-HL095122, P01-GM066730, and K99-HL121160.

## References

- Agarwal B, Camara AK, Stowe DF, Bosnjak ZJ, Dash RK (2012) Enhanced charge-independent mitochondrial free Ca<sup>2+</sup> and attenuated ADP-induced NADH oxidation by isoflurane: implications for cardioprotection. *Biochim Biophys Acta* 1817(3):453–465. doi:10.1016/j.bbabi.2011.11.011 CrossRef
- Agarwal B, Dash RK, Stowe DF, Bosnjak ZJ, Camara AK (2014) Isoflurane modulates cardiac mitochondrial bioenergetics by selectively attenuating respiratory complexes. *Biochim Biophys Acta* 1837(3):354–365. doi:10.1016/j.bbabi.2013.11.006
- Aldakkak M, Camara AK, Heisner JS, Yang M, Stowe DF (2011) Ranolazine reduces Ca<sup>2+</sup> overload and oxidative stress and improves mitochondrial integrity to protect against ischemia reperfusion injury in

- isolated hearts. *Pharmacol Res* 64(4):381–392.  
doi:10.1016/j.phrs.2011.06.018
- Aldakkak M, Stowe DF, Dash RK, Camara AK (2013) Mitochondrial handling of excess  $\text{Ca}^{2+}$  is substrate-dependent with implications for reactive oxygen species generation. *Free Radic Biol Med* 56:193–203.  
doi:10.1016/j.freeradbiomed.2012.09.020
- An J, Varadarajan SG, Camara A, Chen Q, Novalija E, Gross GJ, et al. (2001a) Blocking  $\text{Na}^{+}/\text{H}^{+}$  exchange reduces  $[\text{Na}^{+}]_i$  and  $[\text{Ca}^{2+}]_i$  load after ischemia and improves function in intact hearts. *Am J Physiol Heart Circ Physiol* 281(6):H2398–H2409
- An J, Varadarajan SG, Novalija E, Stowe DF (2001b) Ischemic and anesthetic preconditioning reduces cytosolic  $[\text{Ca}^{2+}]$  and improves  $\text{Ca}^{2+}$  responses in intact hearts. *Am J Physiol Heart Circ Physiol* 281(4):H1508–H1523
- Baughman JM, Perocchi F, Girgis HS, Plovanich M, Belcher-Timme CA, Sancak Y, et al. (2011) Integrative genomics identifies MCU as an essential component of the mitochondrial calcium uniporter. *Nature* 476(7360):341–345. doi:10.1038/nature10234 CrossRef
- Bazil JN, Dash RK (2011) A minimal model for the mitochondrial rapid mode of  $\text{Ca}^{2+}$  uptake mechanism. *PLoS One* 6(6):e21324.  
doi:10.1371/journal.pone.0021324 CrossRef
- Bazil JN, Blomeyer CA, Pradhan RK, Camara AK, Dash RK (2013) Modeling the calcium sequestration system in isolated guinea pig cardiac mitochondria. *J Bioenerg Biomembr* 45(3):177–188.  
doi:10.1007/s10863-012-9488-2
- Beutner G, Sharma VK, Giovannucci DR, Yule DI, Sheu SS (2001) Identification of a ryanodine receptor in rat heart mitochondria. *J Biol Chem* 276(24):21482–21488. doi:10.1074/jbc.M101486200
- Blomeyer CA, Bazil JN, Stowe DF, Pradhan RK, Dash RK, Camara AK (2013) Dynamic buffering of mitochondrial  $\text{Ca}^{2+}$  during  $\text{Ca}^{2+}$  uptake and  $\text{Na}^{+}$ -induced  $\text{Ca}^{2+}$  release. *J Bioenerg Biomembr* 45(3):189–202.  
doi:10.1007/s10863-012-9483-7
- Boelens AD, Pradhan RK, Blomeyer CA, Camara AK, Dash RK, Stowe DF (2013) Extra-matrix  $\text{Mg}^{2+}$  limits  $\text{Ca}^{2+}$  uptake and modulates  $\text{Ca}^{2+}$  uptake-independent respiration and redox state in cardiac isolated mitochondria. *J Bioenerg Biomembr* 45(3):203–218.  
doi:10.1007/s10863-013-9500-5
- Boyman L, Williams GS, Khananshvili D, Sekler I, Lederer WJ (2013) NCLX: the mitochondrial sodium calcium exchanger. *J Mol Cell Cardiol* 59:205–213. doi:10.1016/j.yjmcc.2013.03.012
- Boyman L, Chikando AC, Williams GS, Khairallah RJ, Kettlewell S, Ward CW, et al. (2014) Calcium movement in cardiac mitochondria. *Biophys J* 107(6):1289–1301. doi:10.1016/j.bpj.2014.07.045



- Bradford MM (1976) A rapid and sensitive method for the quantitation of microgram quantities of protein utilizing the principle of protein-dye binding. *Anal Biochem* 72:248–254
- Brierley GP, Bachmann E, Green DE (1962) Active transport of inorganic phosphate and magnesium ions by beef heart mitochondria. *Proc Natl Acad Sci U S A* 48:1928–1935
- Brierley G, Murer E, Bachmann E, Green DE (1963) Studies on ion transport. II. The accumulation of inorganic phosphate and magnesium ions by heart mitochondria. *J Biol Chem* 238:3482–3489
- Brierley GP, Murer E, O'Brien RL (1964) Studies on ion transport. Vi. The accumulation of  $Mg^{2+}$  by heart mitochondria in the absence of inorganic phosphate. *Biochim Biophys Acta* 88:645–647
- Buntinas L, Gunter KK, Sparagna GC, Gunter TE (2001) The rapid mode of calcium uptake into heart mitochondria (RaM): comparison to RaM in liver mitochondria. *Biochim Biophys Acta* 1504(2–3):248–261
- Cai X, Lytton J (2004) Molecular cloning of a sixth member of the  $K^{+}$ -dependent  $Na^{+}/Ca^{2+}$  exchanger gene family, NCKX6. *J Biol Chem* 279(7):5867–5876. doi:10.1074/jbc.M310908200
- Carafoli E (2010) The fateful encounter of mitochondria with calcium: how did it happen? *Biochim Biophys Acta* 1797(6–7):595–606. doi:10.1016/j.bbabbio.2010.03.024
- Chalmers S, Nicholls DG (2003) The relationship between free and total calcium concentrations in the matrix of liver and brain mitochondria. *J Biol Chem* 278(21):19062–19070. doi:10.1074/jbc.M212661200
- Csordas G, Golenar T, Seifert EL, Kamer KJ, Sancak Y, Perocchi F, et al. (2013) MICU1 controls both the threshold and cooperative activation of the mitochondrial  $Ca^{2+}$  uniporter. *Cell Metab* 17(6):976–987. doi:10.1016/j.cmet.2013.04.020
- De Stefani D, Raffaello A, Teardo E, Szabo I, Rizzuto R (2011) A forty-kilodalton protein of the inner membrane is the mitochondrial calcium uniporter. *Nature* 476(7360):336–340. doi:10.1038/nature10230
- Dedkova EN, Blatter LA (2013) Calcium signaling in cardiac mitochondria. *J Mol Cell Cardiol* 58:125–133. doi:10.1016/j.yjmcc.2012.12.021
- Dorn 2nd GW, Maack C (2013) SR and mitochondria: calcium cross-talk between kissing cousins. *J Mol Cell Cardiol* 55:42–49. doi:10.1016/j.yjmcc.2012.07.015
- Douban S, Brodsky MA, Whang DD, Whang R (1996) Significance of magnesium in congestive heart failure. *Am Heart J* 132(3):664–671
- Greenawalt JW, Rossi CS, Lehninger AL (1964) Effect of active accumulation of calcium and phosphate ions on the structure of rat liver mitochondria. *J Cell Biol* 23:21–38

- Grynkiewicz G, Poenie M, Tsien RY (1985) A new generation of  $\text{Ca}^{2+}$  indicators with greatly improved fluorescence properties. *J Biol Chem* 260(6):3440–3450
- Gunter TE, Buntinas L, Sparagna GC, Gunter KK (1998) The  $\text{Ca}^{2+}$  transport mechanisms of mitochondria and  $\text{Ca}^{2+}$  uptake from physiological-type  $\text{Ca}^{2+}$  transients. *Biochim Biophys Acta* 1366(1–2):5–15
- Harrington JL, Murphy E (2015) The mitochondrial calcium uniporter: mice can live and die without it. *J Mol Cell Cardiol* 78:46–53. doi:10.1016/j.yjmcc.2014.10.013
- Haumann J, Dash RK, Stowe DF, Boelens AD, Beard DA, Camara AK (2010) Mitochondrial free  $[\text{Ca}^{2+}]$  increases during ATP/ADP antiport and ADP phosphorylation: exploration of mechanisms. *Biophys J* 99(4):997–1006. doi:10.1016/j.bpj.2010.04.069
- Huser J, Blatter LA, Sheu SS (2000) Mitochondrial calcium in heart cells: beat-to-beat oscillations or slow integration of cytosolic transients? *J Bioenerg Biomembr* 32(1):27–33
- Kamer KJ, Mootha VK (2014) MICU1 and MICU2 play nonredundant roles in the regulation of the mitochondrial calcium uniporter. *EMBO Rep* 15(3):299–307. doi:10.1002/embr.201337946
- Kirichok Y, Krapivinsky G, Clapham DE (2004) The mitochondrial calcium uniporter is a highly selective ion channel. *Nature* 427(6972):360–364. doi:10.1038/nature02246
- Kolte D, Vijayaraghavan K, Khera S, Sica DA, Frishman WH (2014) Role of magnesium in cardiovascular diseases. *Cardiol Rev* 22(4):182–192. doi:10.1097/CRD.0000000000000003
- Kristian T, Pivovarova NB, Fiskum G, Andrews SB (2007) Calcium-induced precipitate formation in brain mitochondria: composition, calcium capacity, and retention. *J Neurochem* 102(4):1346–1356. doi:10.1111/j.1471-4159.2007.04626.x
- Kwong JQ, Lu X, Correll RN, Schwanekamp JA, Vagnozzi RJ, Sargent MA, et al. (2015) The mitochondrial calcium uniporter selectively matches metabolic output to acute contractile stress in the heart. *Cell Rep* 12(1):15–22. doi:10.1016/j.celrep.2015.06.002
- Levitsky DO, Takahashi M (2013) Interplay of  $\text{Ca}^{2+}$  and  $\text{Mg}^{2+}$  in sodium-calcium exchanger and in other  $\text{Ca}^{2+}$ -binding proteins: magnesium, watchdog that blocks each turn if able. *Adv Exp Med Biol* 961:65–78. doi:10.1007/978-1-4614-4756-6\_7
- Lu X, Ginsburg KS, Kettlewell S, Bossuyt J, Smith GL, Bers DM (2013) Measuring local gradients of intramitochondrial  $[\text{Ca}^{2+}]$  in cardiac myocytes during sarcoplasmic reticulum  $\text{Ca}^{2+}$  release. *Circ Res* 112(3):424–431. doi:10.1161/CIRCRESAHA.111.300501
- Luongo TS, Lambert JP, Yuan A, Zhang X, Gross P, Song J, et al. (2015) The mitochondrial calcium uniporter matches energetic supply with cardiac

- workload during stress and modulates permeability transition. *Cell Rep* 12(1):23–34. doi:10.1016/j.celrep.2015.06.017
- Mallilankaraman K, Doonan P, Cardenas C, Chandramoorthy HC, Muller M, Miller R, et al. (2012) MICU1 is an essential gatekeeper for MCU-mediated mitochondrial Ca<sup>2+</sup> uptake that regulates cell survival. *Cell* 151(3):630–644. doi:10.1016/j.cell.2012.10.011
- Marchi S, Pinton P (2014) The mitochondrial calcium uniporter complex: molecular components, structure and physiopathological implications. *J Physiol* 592(Pt 5):829–839. doi:10.1113/jphysiol.2013.268235
- Nicholls DG (2005) Mitochondria and calcium signaling. *Cell Calcium* 38(3–4):311–317. doi:10.1016/j.ceca.2005.06.011
- O'Rourke B, Blatter LA (2009) Mitochondrial Ca<sup>2+</sup> uptake: tortoise or hare? *J Mol Cell Cardiol* 46(6):767–774. doi:10.1016/j.yjmcc.2008.12.011
- Palty R, Ohana E, Hershinkel M, Volokita M, Elgazar V, Beharier O, et al. (2004) Lithium-calcium exchange is mediated by a distinct potassium-independent sodium-calcium exchanger. *J Biol Chem* 279(24):25234–25240. doi:10.1074/jbc.M401229200
- Pan X, Liu J, Nguyen T, Liu C, Sun J, Teng Y, et al. (2013) The physiological role of mitochondrial calcium revealed by mice lacking the mitochondrial calcium uniporter. *Nat Cell Biol* 15(12):1464–1472. doi:10.1038/ncb2868
- Patron M, Checchetto V, Raffaello A, Teardo E, Vecellio Reane D, Mantoan M, et al. (2014) MICU1 and MICU2 finely tune the mitochondrial Ca<sup>2+</sup> uniporter by exerting opposite effects on MCU activity. *Mol Cell* 53(5):726–737. doi:10.1016/j.molcel.2014.01.013
- Pradhan RK, Qi F, Beard DA, Dash RK (2011) Characterization of Mg<sup>2+</sup> inhibition of mitochondrial Ca<sup>2+</sup> uptake by a mechanistic model of mitochondrial Ca<sup>2+</sup> uniporter. *Biophys J* 101(9):2071–2081. doi:10.1016/j.bpj.2011.09.029
- Rasola A, Bernardi P (2011) Mitochondrial permeability transition in Ca<sup>2+</sup>-dependent apoptosis and necrosis. *Cell Calcium* 50(3):222–233. doi:10.1016/j.ceca.2011.04.007
- Rhodes SS, Ropella KM, Audi SH, Camara AK, Kevin LG, Pagel PS, et al. (2003) Cross-bridge kinetics modeled from myoplasmic [Ca<sup>2+</sup>] and LV pressure at 17 degrees C and after 37 degrees C and 17 degrees C ischemia. *Am J Physiol Heart Circ Physiol* 284(4):H1217–H1229. doi:10.1152/ajpheart.00816.2002
- Sareen D, Darjatmoko SR, Albert DM, Polans AS (2007) Mitochondria, calcium, and calpain are key mediators of resveratrol-induced apoptosis in breast cancer. *Mol Pharmacol* 72(6):1466–1475. doi:10.1124/mol.107.039040

- Scaduto RC, Grotyohann LW (1999) Measurement of mitochondrial membrane potential using fluorescent rhodamine derivatives. *Biophys J* 76(1 Pt 1):469–477. doi:10.1016/S0006-3495(99)77214-0
- Sedova M, Dedkova EN, Blatter LA (2006) Integration of rapid cytosolic  $\text{Ca}^{2+}$  signals by mitochondria in cat ventricular myocytes. *Am J Physiol Cell Physiol* 291(5):C840–C850. doi:10.1152/ajpcell.00619.2005
- Seelig M (1989) Cardiovascular consequences of magnesium deficiency and loss: pathogenesis, prevalence and manifestations—magnesium and chloride loss in refractory potassium repletion. *Am J Cardiol* 63(14):4G–21G
- Sparagna GC, Gunter KK, Sheu SS, Gunter TE (1995) Mitochondrial calcium uptake from physiological-type pulses of calcium. A description of the rapid uptake mode. *J Biol Chem* 270(46):27510–27515
- Szabadkai G, Duchen MR (2008) Mitochondria: the hub of cellular  $\text{Ca}^{2+}$  signaling. *Physiology (Bethesda)* 23:84–94. doi:10.1152/physiol.00046.2007
- Tarasov AI, Griffiths EJ, Rutter GA (2012) Regulation of ATP production by mitochondrial  $\text{Ca}^{2+}$ . *Cell Calcium* 52(1):28–35. doi:10.1016/j.ceca.2012.03.003
- Tewari SG, Camara AK, Stowe DF, Dash RK (2014) Computational analysis of  $\text{Ca}^{2+}$  dynamics in isolated cardiac mitochondria predicts two distinct modes of  $\text{Ca}^{2+}$  uptake. *J Physiol* 592(Pt 9):1917–1930. doi:10.1113/jphysiol.2013.268847
- Thomas RS, Greenawalt JW (1968) Microincineration, electron microscopy, and electron diffraction of calcium phosphate-loaded mitochondria. *J Cell Biol* 39(1):55–76
- Varadarajan SG, An J, Novalija E, Smart SC, Stowe DF (2001) Changes in  $[\text{Na}^+]_i$ , compartmental  $[\text{Ca}^{2+}]_i$ , and NADH with dysfunction after global ischemia in intact hearts. *Am J Physiol Heart Circ Physiol* 280(1):H280–H293
- Vasington FD, Murphy JV (1962)  $\text{Ca}^{2+}$  ion uptake by rat kidney mitochondria and its dependence on respiration and phosphorylation. *J Biol Chem* 237:2670–2677
- Wei AC, Liu T, Winslow RL, O'Rourke B (2012) Dynamics of matrix-free  $\text{Ca}^{2+}$  in cardiac mitochondria: two components of  $\text{Ca}^{2+}$  uptake and role of phosphate buffering. *J Gen Physiol* 139(6):465–478. doi:10.1085/jgp.201210784
- Wingrove DE, Gunter TE (1986) Kinetics of mitochondrial calcium transport. II. A kinetic description of the sodium-dependent calcium efflux mechanism of liver mitochondria and inhibition by ruthenium red and by tetraphenylphosphonium. *J Biol Chem* 261(32):15166–15171
- Wu LN, Genge BR, Wuthier RE (2008) Analysis and molecular modeling of the formation, structure, and activity of the phosphatidylserine-calcium-

phosphate complex associated with biomineralization. *J Biol Chem* 283(7):3827–3838. doi:10.1074/jbc.M707653200

Wu LN, Genge BR, Wuthier RE (2009) Differential effects of zinc and magnesium ions on mineralization activity of phosphatidylserine calcium phosphate complexes. *J Inorg Biochem* 103(7):948–962. doi:10.1016/j.jinorgbio.2009.04.004

Wu Y, Rasmussen TP, Koval OM, Joiner ML, Hall DD, Chen B, et al. (2015) The mitochondrial uniporter controls fight or flight heart rate increases. *Nat Commun* 6:6081. doi:10.1038/ncomms7081

## Figures and Tables

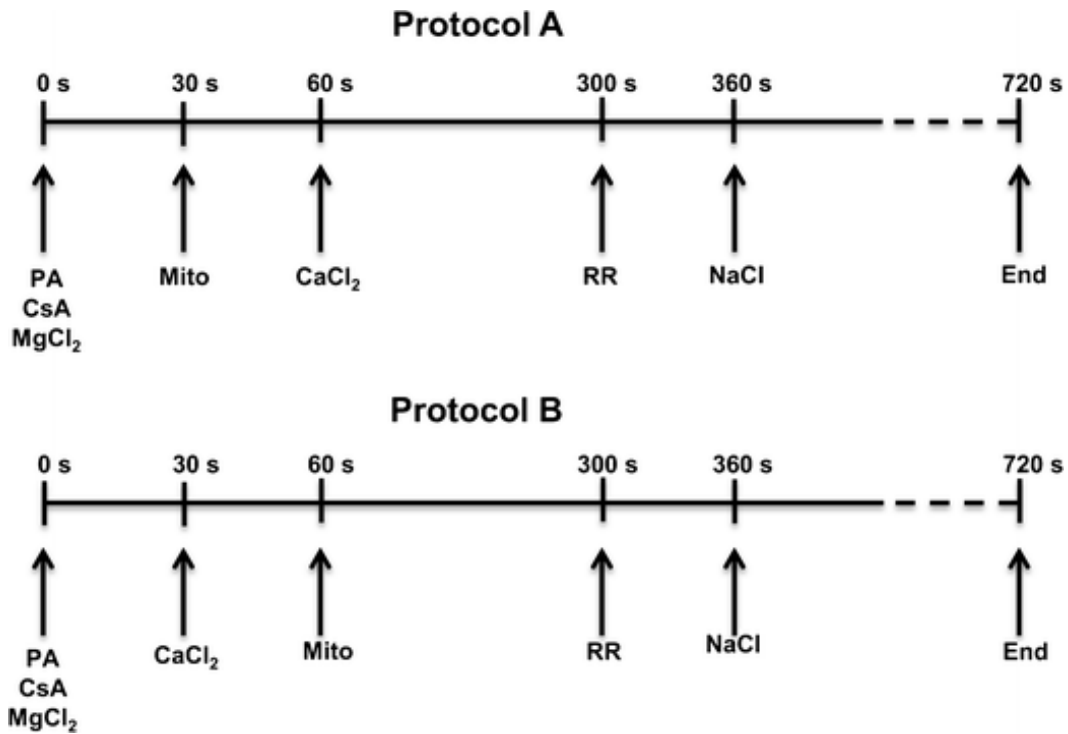


**Fig. 1:** Timelines show the two experimental protocols used to characterize and quantify mitochondrial Ca<sup>2+</sup> handling (influx, efflux, sequestration) in isolated guinea pig cardiac mitochondria. In protocol A, mitochondria were added to the experimental buffer before CaCl<sub>2</sub> was added. In protocol B, mitochondria were added to respiration buffer with CaCl<sub>2</sub> already present. All other additions were identical between protocols. 40 μM EGTA was present in all the experimental buffers; 0.5 μM CsA was added to all mitochondrial suspensions. Inset axes are the same as the main figure panels

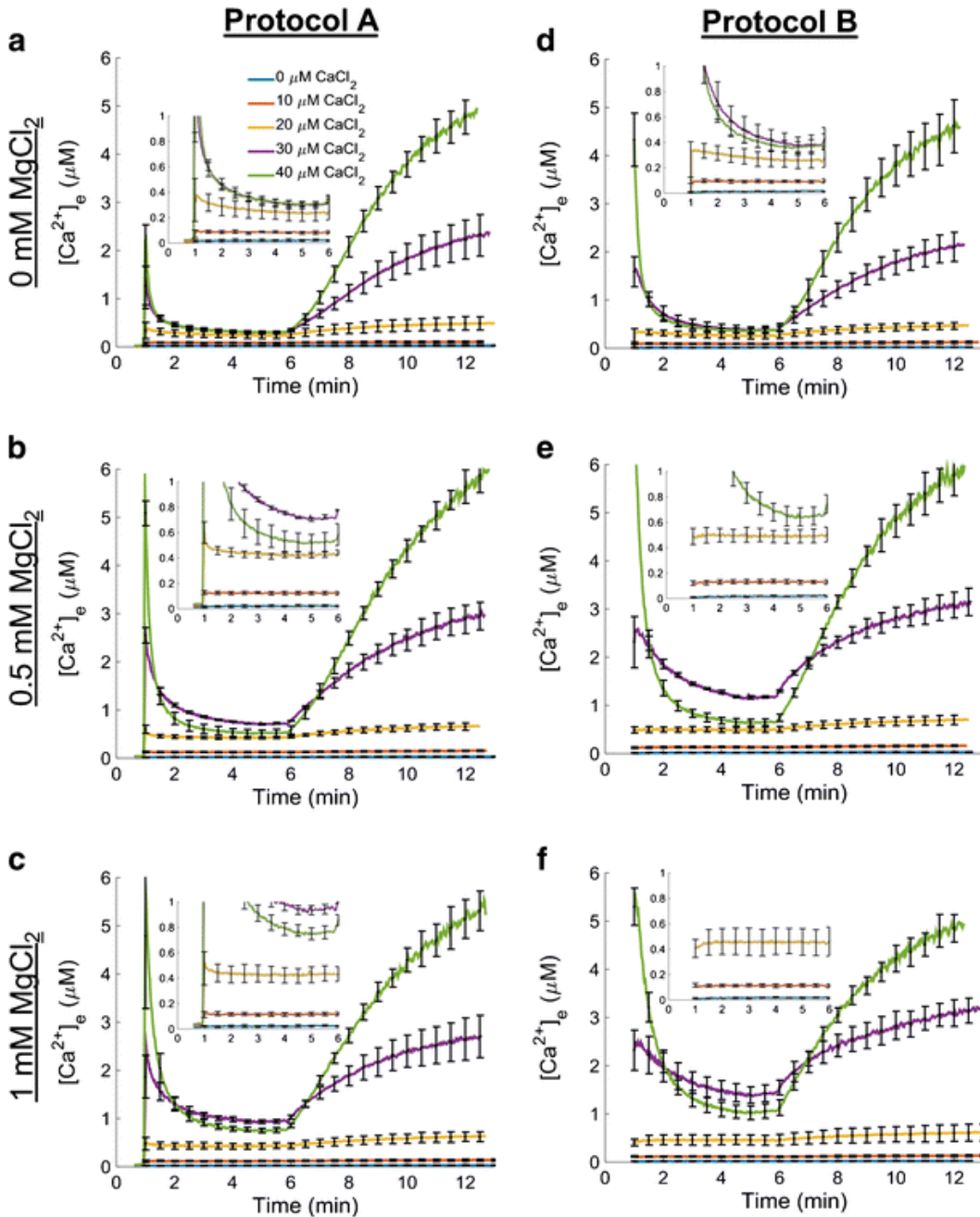


**Fig. 2:** Extra-matrix free Ca<sup>2+</sup> ([Ca<sup>2+</sup>]<sub>e</sub>) dynamics. Ca<sup>2+</sup> uptake and Ca<sup>2+</sup> release for each combination of CaCl<sub>2</sub> and MgCl<sub>2</sub> concentrations are shown using the protocol depicted in Fig. 1. CaCl<sub>2</sub> was added to respiring mitochondrial suspension (left column; protocol A) or mitochondria were added to the buffer containing a given CaCl<sub>2</sub> concentration (right column; protocol B) at 60 s followed by ruthenium red (RR) at 300 s and NaCl at 360 s. The results for protocol A are shown in the left column and the results for protocol B are shown in the right column. Each row corresponds to the buffer MgCl<sub>2</sub> indicated on the left of each row. Insets show [Ca<sup>2+</sup>]<sub>e</sub> dynamics for 0, 10, and 20 μM CaCl<sub>2</sub> in more detail. The axes are the same as the axes in the main figure panels. Error bars signify standard error of the mean

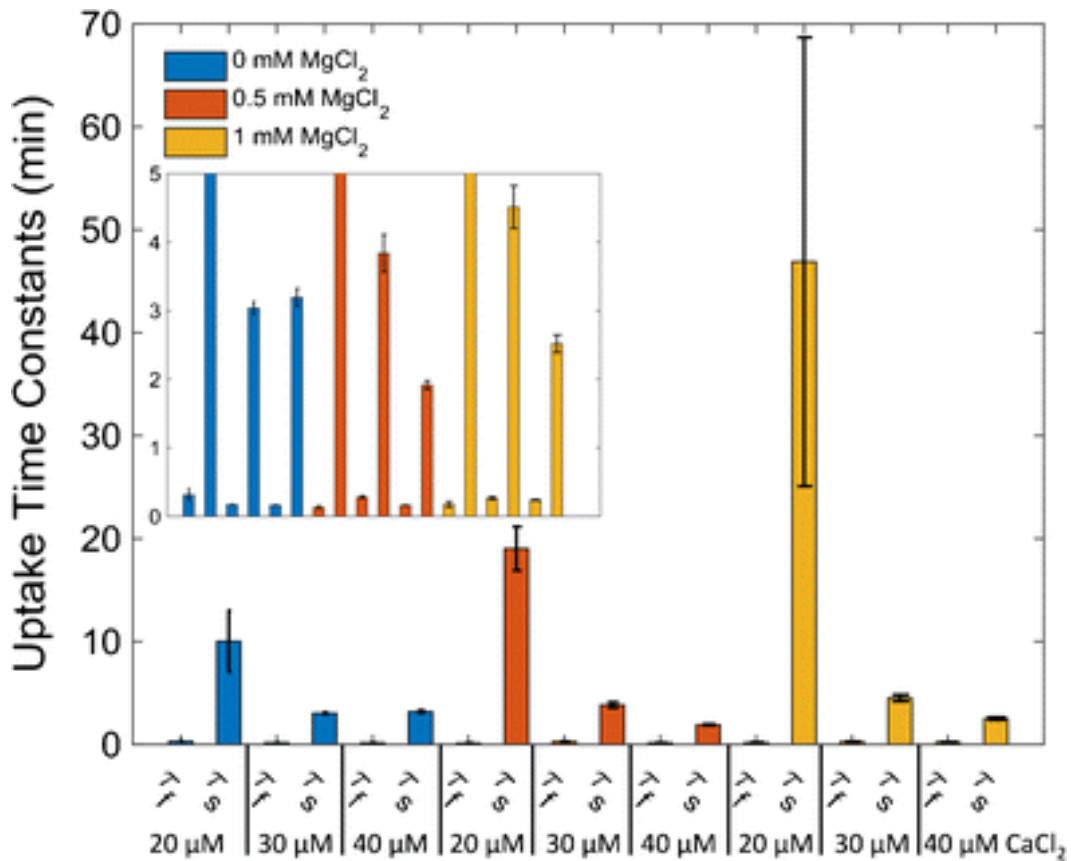


**Fig. 3:** Two modes of Ca<sup>2+</sup> uptake. For CaCl<sub>2</sub> concentrations of 20 μM and greater, a double exponential function was fit between 65 s and 150 s to the [Ca<sup>2+</sup>]<sub>e</sub> dynamics observed in protocol A (Fig. 2). The fit time constants show that there was a fast and slow component of Ca<sup>2+</sup> uptake associated with each bolus of CaCl<sub>2</sub> administered. The inset axes labels are the same as the main figure panel. Error bars signify propagated standard deviations

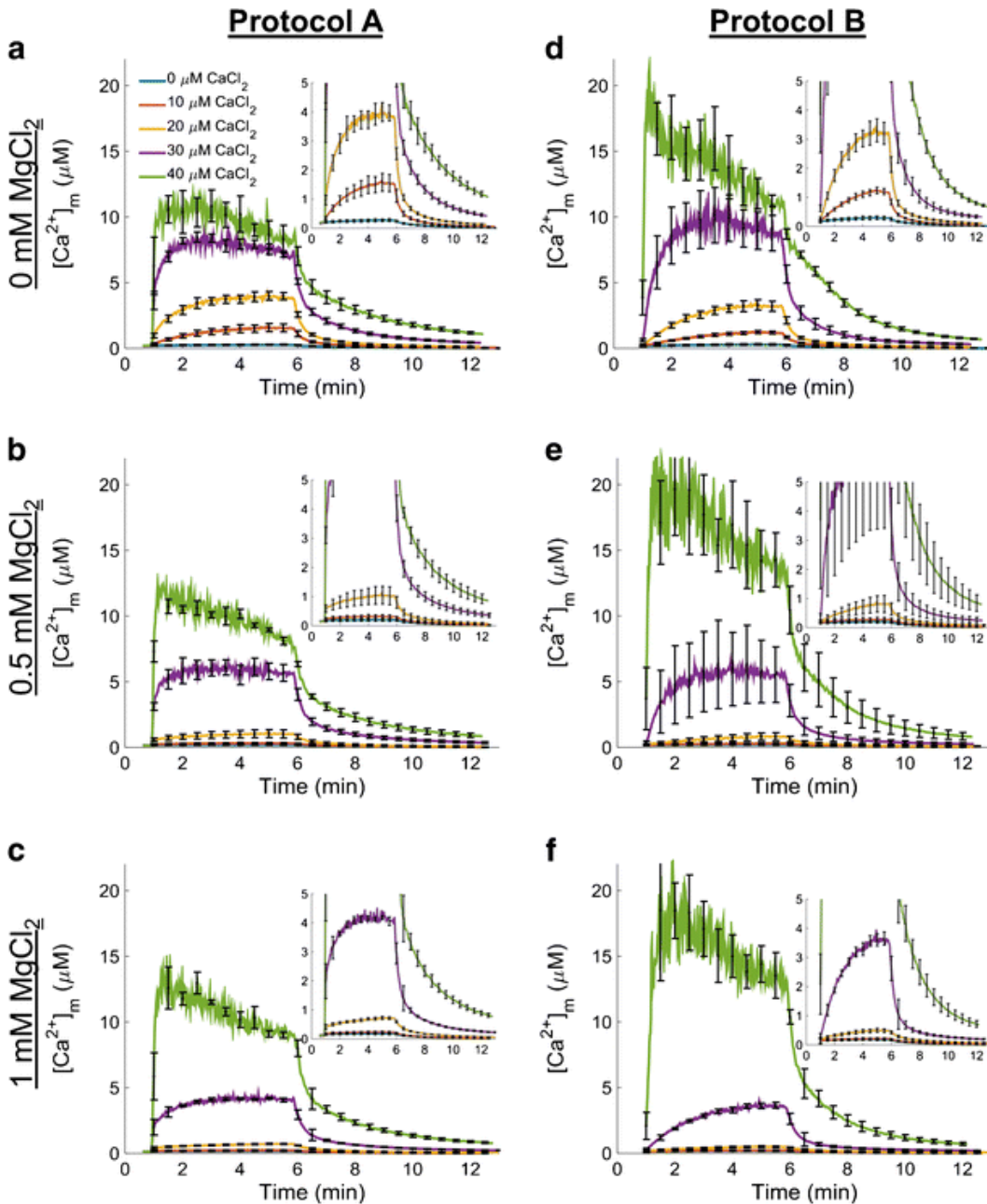


**Fig. 4:** Matrix free  $\text{Ca}^{2+}$  ( $[\text{Ca}^{2+}]_m$ ) dynamics.  $\text{Ca}^{2+}$  uptake and  $\text{Ca}^{2+}$  release for each combination of  $\text{CaCl}_2$  and  $\text{MgCl}_2$  concentrations are shown using the protocol depicted in Fig. 1.  $\text{CaCl}_2$  was added to the respiring mitochondrial suspension (left column; protocol A) or mitochondria were added to the buffer containing a given  $\text{CaCl}_2$  concentration (right column; protocol B) at 60 s followed by ruthenium red (RR) at 300 s and NaCl at 360 s. The results for protocol A are shown in the left column and the results for protocol B in the right column. In protocol B when  $\text{CaCl}_2$  was 40  $\mu\text{M}$ , the fluorescent signal was close to  $R_{\text{max}}$ , so the calculated  $[\text{Ca}^{2+}]_m$  is likely an overestimation of the true value of  $[\text{Ca}^{2+}]_m$ . Each row corresponds to the buffer  $\text{MgCl}_2$  indicated on the left of each row. Insets show  $[\text{Ca}^{2+}]_m$  dynamics for 0, 10, and 20  $\mu\text{M}$



CaCl<sub>2</sub> in more detail. The axes are the same as the axes in the main figure panels. Error bars signify standard error of the mean

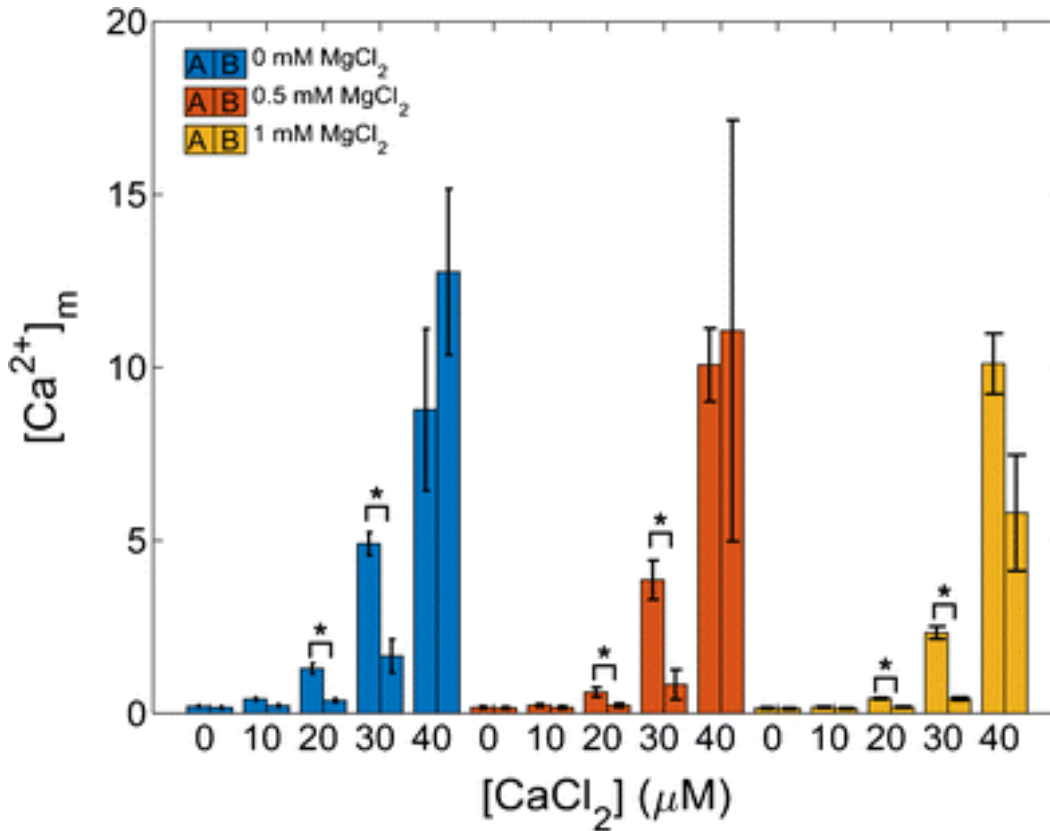


**Fig. 5:** Ca<sup>2+</sup> uptake by mitochondria. The amount of Ca<sup>2+</sup> uptake by mitochondria depends on method of CaCl<sub>2</sub> delivery. The bar plots show  $[Ca^{2+}]_m$  just after addition of CaCl<sub>2</sub> to mitochondria (protocol A, left bar) or after addition of mitochondria to buffer containing CaCl<sub>2</sub> (protocol B, right bar). These data correspond to a time of approximately 65 s. For all 20 and 30  $\mu M$  CaCl<sub>2</sub> conditions, the rate of Ca<sup>2+</sup> uptake in protocol A was significantly different from that of protocol B ( $p \leq 0.05$ ) for most of the  $[CaCl_2]$  and even in the presence of Mg<sup>2+</sup>. Error bars signify standard error of the mean

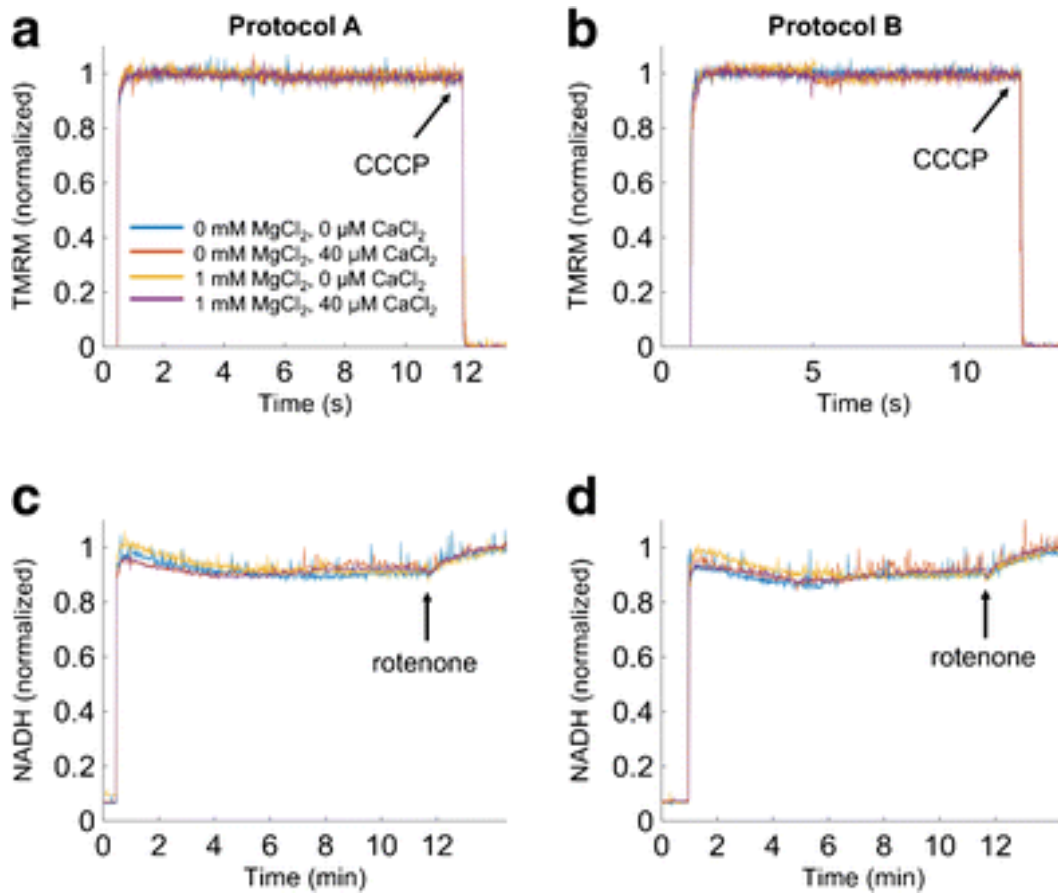


**Fig. 6:**  $\Delta\Psi_m$  and NADH dynamics. The bioenergetics responses during protocols A and B were monitored in parallel using the  $\Delta\Psi_m$  sensitive dye TMRM and NADH autofluorescence. Traces are individual recordings. In averaged data there were no significant differences between the two MgCl<sub>2</sub> and CaCl<sub>2</sub> groups. The increases in signals mark the addition of mitochondria at 30 s (protocol A) and at 60 s (protocol B). The number of experimental groups was reduced to consist of only 0 and 1 mM MgCl<sub>2</sub> and 0 and 40 μM CaCl<sub>2</sub>

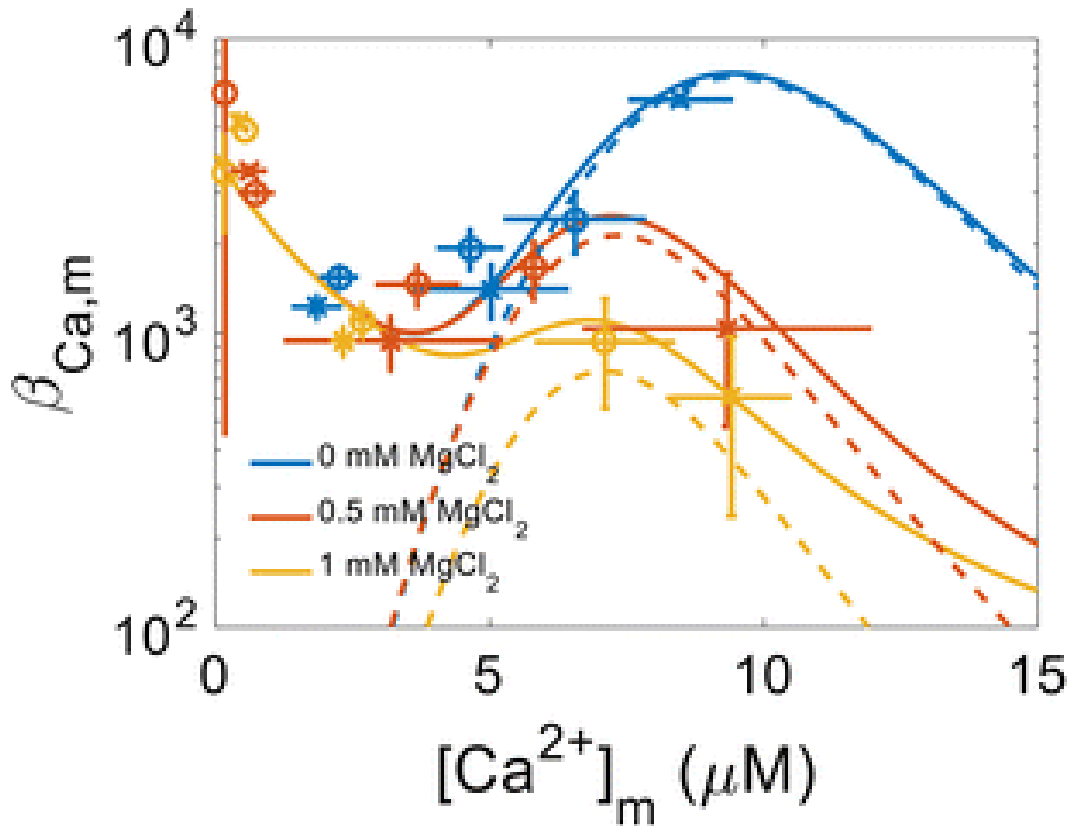


**Fig. 7:** Mitochondrial  $\text{Ca}^{2+}$  buffering power. The  $\text{Ca}^{2+}$  sequestration system consists of at least two classes of buffers that bind  $\text{Ca}^{2+}$  with a differential affinity and capacity. Class 1 buffers are of the prototypical type whereby a single  $\text{Ca}^{2+}$  ion binds to a single site in an uncooperative manner. Class 2 buffers are atypical and bind multiple  $\text{Ca}^{2+}$  ions in a cooperative fashion. Class 1 buffers are not affected by  $\text{Mg}^{2+}$ ; however, in the presence of  $\text{Mg}^{2+}$ , both the binding capacity and affinity of the Class 2 buffers are compromised. The blue, yellow and red colors correspond to the added 0 mM  $\text{MgCl}_2$ , 0.5 mM  $\text{MgCl}_2$  and 1 mM  $\text{MgCl}_2$  conditions, respectively. The circles (●) and x's (x) represent rates obtained using the data from Protocols A and B, respectively. The lines correspond to model simulations of the two classes of  $\text{Ca}^{2+}$  buffers using Eq. 2 with the parameters listed in Table 1. Error bars signify propagated standard deviations. Dashed lines represent contributions to mitochondrial buffering power from the class 2 buffers only

**Table 1:** Mitochondrial Ca<sup>2+</sup> sequestration system model parameters

| Parameter          | Definition                       | Value              |                         |                       |
|--------------------|----------------------------------|--------------------|-------------------------|-----------------------|
| Class 1            |                                  |                    |                         |                       |
| $[B_{Ca,1}]_{tot}$ | Total Ca <sup>2+</sup> buffer    | 12 mM              |                         |                       |
| $K_{Ca,1}$         | Buffer Ca <sup>2+</sup> affinity | 3 μM               |                         |                       |
| $n_1$              | Hill coefficient                 | 1                  |                         |                       |
| Class 2            |                                  |                    |                         |                       |
|                    |                                  | 0 Mg <sup>2+</sup> | 0.5 mM Mg <sup>2+</sup> | 1 mM Mg <sup>2+</sup> |
| $[B_{Ca,2}]_{tot}$ | Total Ca <sup>2+</sup> buffer    | 8 mM               | 1.8 mM                  | 0.6 mM                |
| $K_{Ca,2}$         | Buffer Ca <sup>2+</sup> affinity | 10 μM              | 7.75 μM                 | 7.5 μM                |
| $n_2$              | Hill coefficient                 | 6                  |                         |                       |

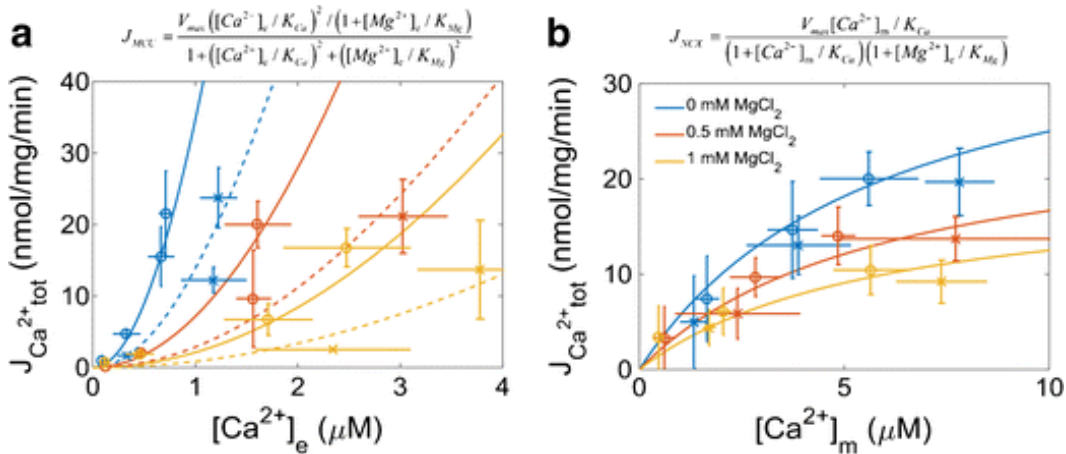


**Fig. 8:** Mg<sup>2+</sup> inhibition of Ca<sup>2+</sup> uptake and extrusion. Panel 8a shows slow mode of Ca<sup>2+</sup> uptake (via MCU) was attenuated by extra-matrix Mg<sup>2+</sup> in the physiological concentration range. The model parameters for the simplified MCU model are:  $V_{max}$ , 900 nmol/mg/min;  $K_{Ca}$ , 6 μM; and  $K_{Mg}$ , 0.3 mM. Solid lines correspond to slow mode of MCU rates observed during protocol A, and dotted lines correspond to the slow mode of MCU rates observed during protocol B. The rates of Ca<sup>2+</sup> uptake in protocol B were approximately 40 % of the rates observed in protocol A. Panel 8b shows buffer Mg<sup>2+</sup> in the physiological range used in this study also affected the rate of Ca<sup>2+</sup> efflux (via mNCE). The model parameters for the simplified NCE are:  $V_{max}$ , 40 nmol/mg/min;  $K_{Ca}$ , 5 μM; and  $K_{Mg}$ , 1 mM. The blue, yellow and red colors correspond to the 0 mM MgCl<sub>2</sub>, 0.5 mM MgCl<sub>2</sub> and 1 mM MgCl<sub>2</sub> conditions, respectively. Extra-matrix [Na<sup>+</sup>] was assumed constant (10 mM) and thus not included in the equation. The circles (●) and x's (x) represent rates obtained using the data from Protocols A and B, respectively. The lines correspond to model simulations with the equations given above their respective panels. Error bars signify propagated standard deviations

## Supplementary Materials

### Mg<sup>2+</sup> differentially regulates two modes of Ca<sup>2+</sup> uptake and Ca<sup>2+</sup> sequestration in isolated cardiac mitochondria

Christoph A. Blomeyer<sup>1\*</sup>, Jason N. Bazil<sup>2-4\*</sup>, David F. Stowe<sup>1,4-6</sup>, Ranjan K. Dash<sup>3-5</sup>, and Amadou K.S. Camara<sup>1,4</sup>

<sup>1</sup>Department of Anesthesiology, Medical College of Wisconsin, Milwaukee, WI 53226, USA

<sup>2</sup>Department of Molecular and Integrative Physiology, University of Michigan, Ann Arbor, MI 48109, USA

<sup>3</sup>Biotechnology and Bioengineering Center, Medical College of Wisconsin, Milwaukee, WI 53226, USA

<sup>4</sup>Department of Physiology, Medical College of Wisconsin, Milwaukee, WI 53226, USA

<sup>5</sup>Department of Biomedical Engineering, Marquette University, Milwaukee, WI 53233, USA

<sup>6</sup>Research Service, Zablocki Veterans Affairs Medical Center, Milwaukee WI 53295, USA

\*These authors equally contributed to the work.

Address for correspondence: Amadou K.S. Camara, Department of Anesthesiology, Medical College of Wisconsin, 8701 Watertown Plank Road, Milwaukee, WI 53226, USA, Phone: (414) 955-5624, Fax: (414) 955-6507, Email: aksc@mcw.edu

## Determination of Ca<sup>2+</sup> K<sub>d</sub> for Fura-4F

The original K<sub>d</sub> for Fura-4F as a marker for intracellular [Ca<sup>2+</sup>] was furnished by the manufacturer, Molecular Probes Inc. (Eugene, OR, USA), and was reported to be approximately 770 nM [Ca<sup>2+</sup>] at pH 7.20 and at 22°C. It is well known that temperature, protein concentration, and pH can influence the apparent K<sub>d</sub> of Ca<sup>2+</sup> dyes (Gryniewicz et al. 1985), including Fura-4F. Therefore, these factors must be considered and accounted for in determining the K<sub>d</sub> for the fluorescent probe under specified experimental conditions. We determined the K<sub>d</sub> for Fura-4F penta-potassium salt (PP) and the acetoxymethyl ethyl ester (AM) version of the probe under our specific experimental conditions using our previous calibration protocol (Boelens et al. 2013) and by measuring the spectral response at different free [Ca<sup>2+</sup>]. For this purpose, we used a Ca<sup>2+</sup> calibration buffer kit #1 provided by Molecular Probes Inc. (MP C-3008), which contained two bottles of 50 ml calibration solution (10 mM K<sub>2</sub>-EGTA and 10 mM Ca-EGTA) with 100 mM KCl and 30 mM MOPS at pH 7.2, conditions that approximate our experimental buffer at 25 °C (room temperature). The two solutions contained free [Ca<sup>2+</sup>] of 0 and 39 μM, which we used to obtain minimal (min) and maximal (max) values of Ca<sup>2+</sup> for calibration. By mixing these two stock solutions in appropriate proportions,

we prepared several solutions with different (known) free  $[Ca^{2+}]$  within the range of 0 to 39  $\mu M$ , given by the formula:

$$\text{Free } [Ca^{2+}] = K_d^{EGTA} [Ca-EGTA]/[K_2-EGTA]$$

Continuous excitation scans ( $\lambda_{ex}$ ) were recorded over the range 290 to 450 nm at a fixed emission ( $\lambda_{em}$ ) 510 nm. To determine the  $K_d$  for Fura-4F AM, isolated mitochondria were loaded with the AM version of the dye and suspended in buffer with different free  $[Ca^{2+}]$ . Ionomycin and CCCP were present to equilibrate  $Ca^{2+}$  and protons (pH), respectively, across the inner mitochondrial membrane. In a separate set of experiments, we determined the  $K_d$  for Fura-4F PP by directly adding the salt form of the dye to the buffer. In this case, to make up for the lack of dye loading, as in the Fura-4F AM situation, mitochondria were incubated with the vehicle for Fura-4F AM, DMSO. No ionomycin or CCCP was added because  $Ca^{2+}$  and protons did not need to be equilibrated. Before adding mitochondria into the buffer, ruthenium red was added to inhibit uptake of  $Ca^{2+}$ . We did these experiments with and without background (NADH autofluorescence) subtraction and observed that the background subtraction had no effect on our results, in the present case of Fura-4F dye. The obtained spectral responses for Fura-4F AM and PP were analyzed and a calibration curve was derived by entering the data in a double log plot (Fig. S1 and Fig S2). Fig. S2 shows the  $Ca^{2+}$  response of the dye is linear with the x-intercept being equal to the log of the apparent  $K_d$  of the dye. The derived  $K_d$  values for the AM and PP version of the dye under our experimental conditions were determined as 890 nM  $[Ca^{2+}]$ . This value (890 nM) rather than the manufacturer's value (770 nM) was used to calculate the  $[Ca^{2+}]_m$  and  $[Ca^{2+}]_e$  in our experiments.

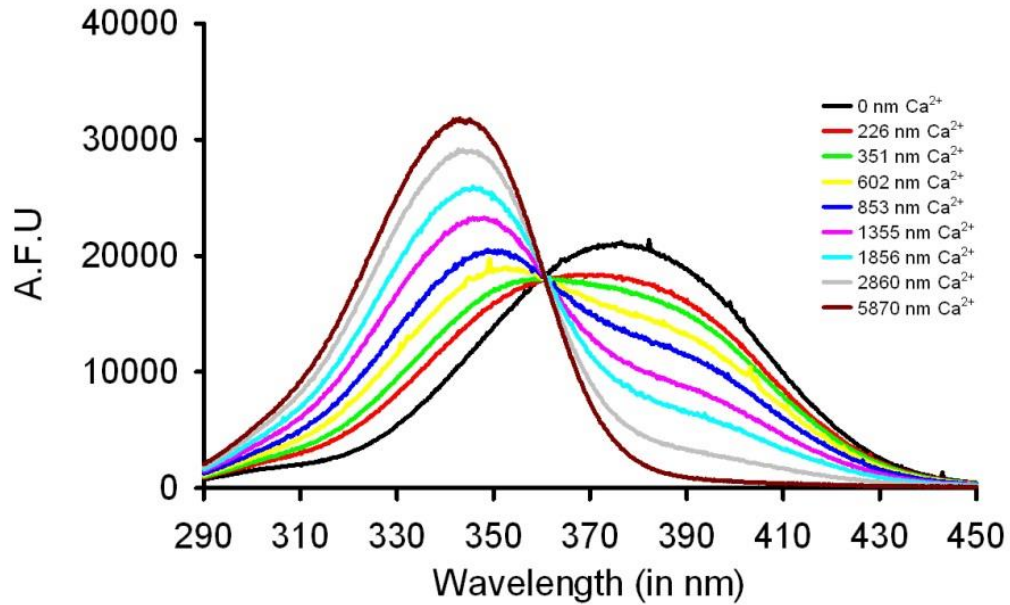


**Fig. S1.** Fluorescence intensities in Arbitrary Fluorescence Units (A.F.U.) were measured at  $\lambda_{em}$  510 nm and R was calculated by dividing  $F_{340}/F_{380}$ . 0  $\mu$ M free  $Ca^{2+}$  was used to determine the ratio when all of the dye was unbound ( $R_{min}$ ) and 39  $\mu$ M free  $Ca^{2+}$  for ratio when all of the dye was bound to  $Ca^{2+}$  ( $R_{max}$ ).

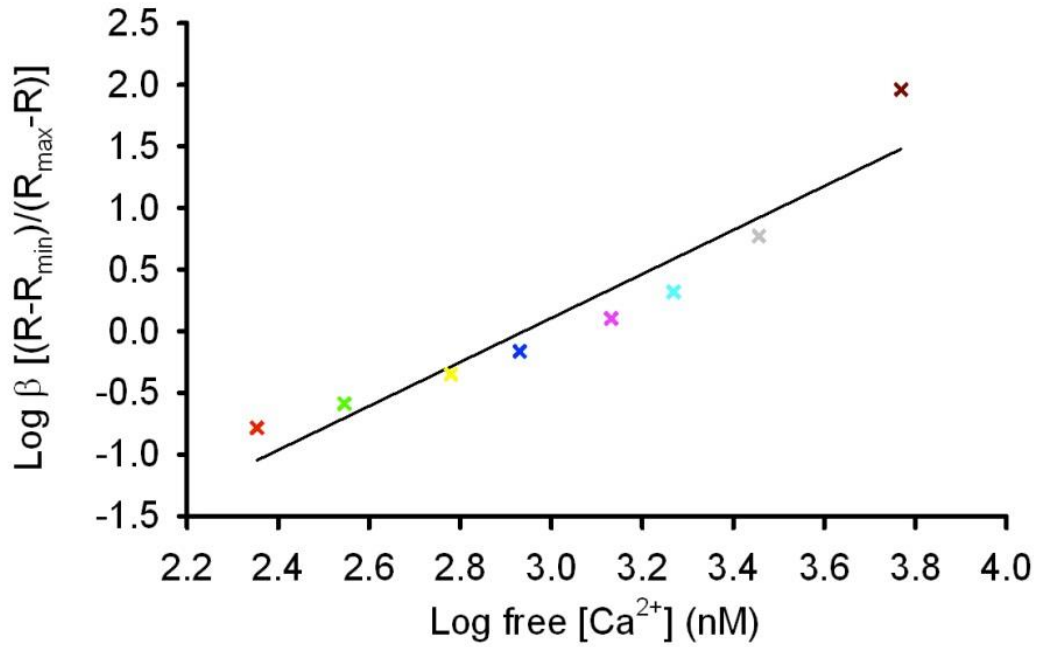


**Fig. S2.** Determination of  $K_d$  for Fura-4F. In a plot of  $\log [Ca^{2+}]$  on the x-axis vs.  $-\log \beta [(R-R_{min})/(R_{max}-R)]$  on the y-axis, the data points formed a straight line with the x-intercept representing the log of the apparent  $K_d$ .



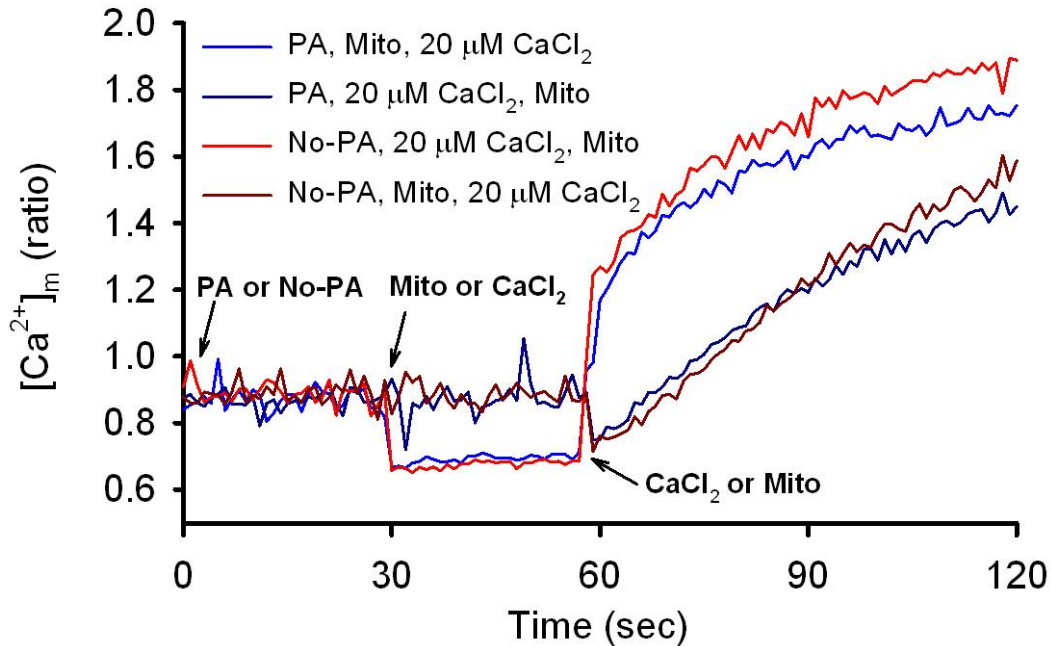


**Fig. S3.** The different modes of  $Ca^{2+}$  uptake are still evident in the absence of exogenous pyruvic acid (PA). When protocol A was used with or without exogenous PA, the fast mode of  $Ca^{2+}$  uptake was observed (light red and light blue lines). And when protocol B was used with or without exogenous PA, only the slow mode was apparent (dark red and dark blue lines).

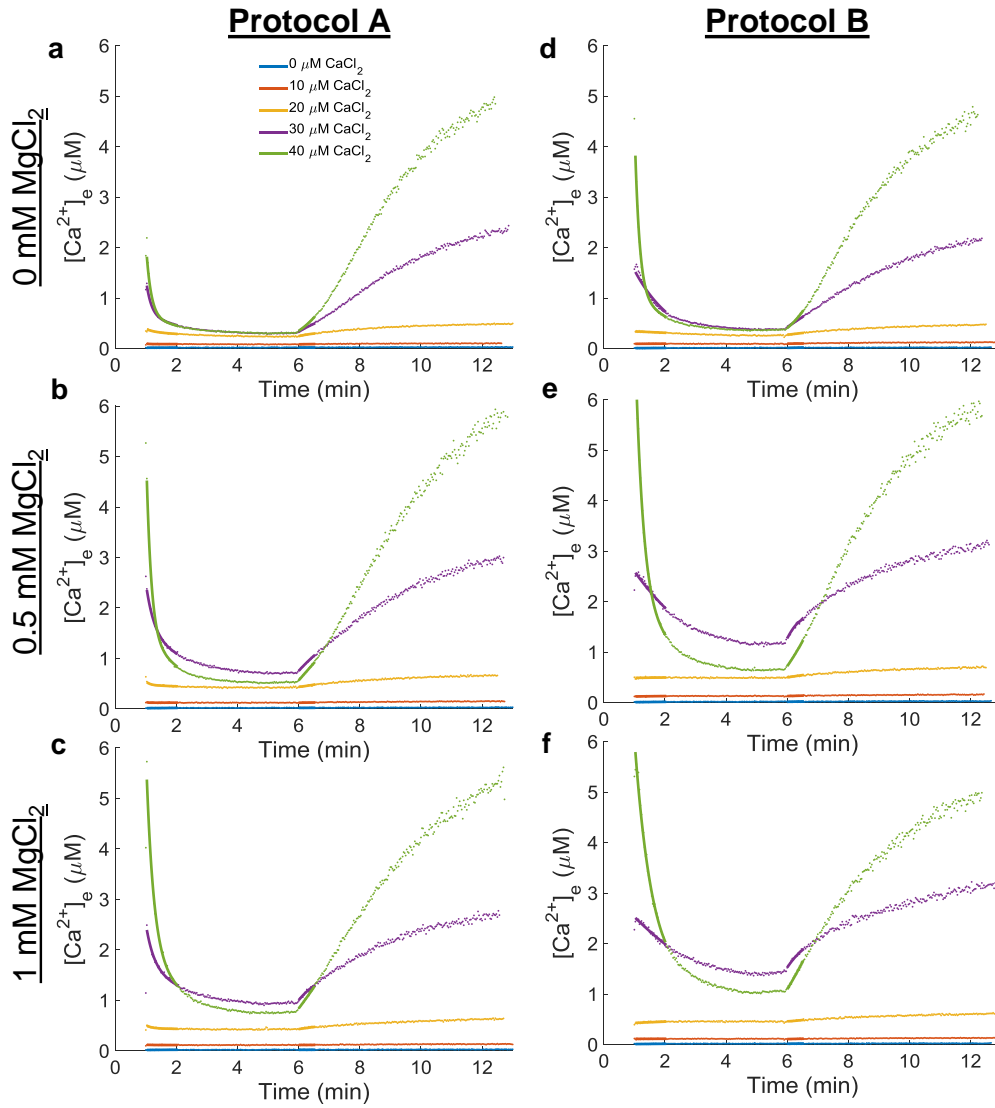


**Fig. S4.** Non-linear trend line fits to the data used to compute extra-matrix Ca<sup>2+</sup> uptake and efflux rates. Layout is identical to that shown in Fig. 2 except no error bars are given.

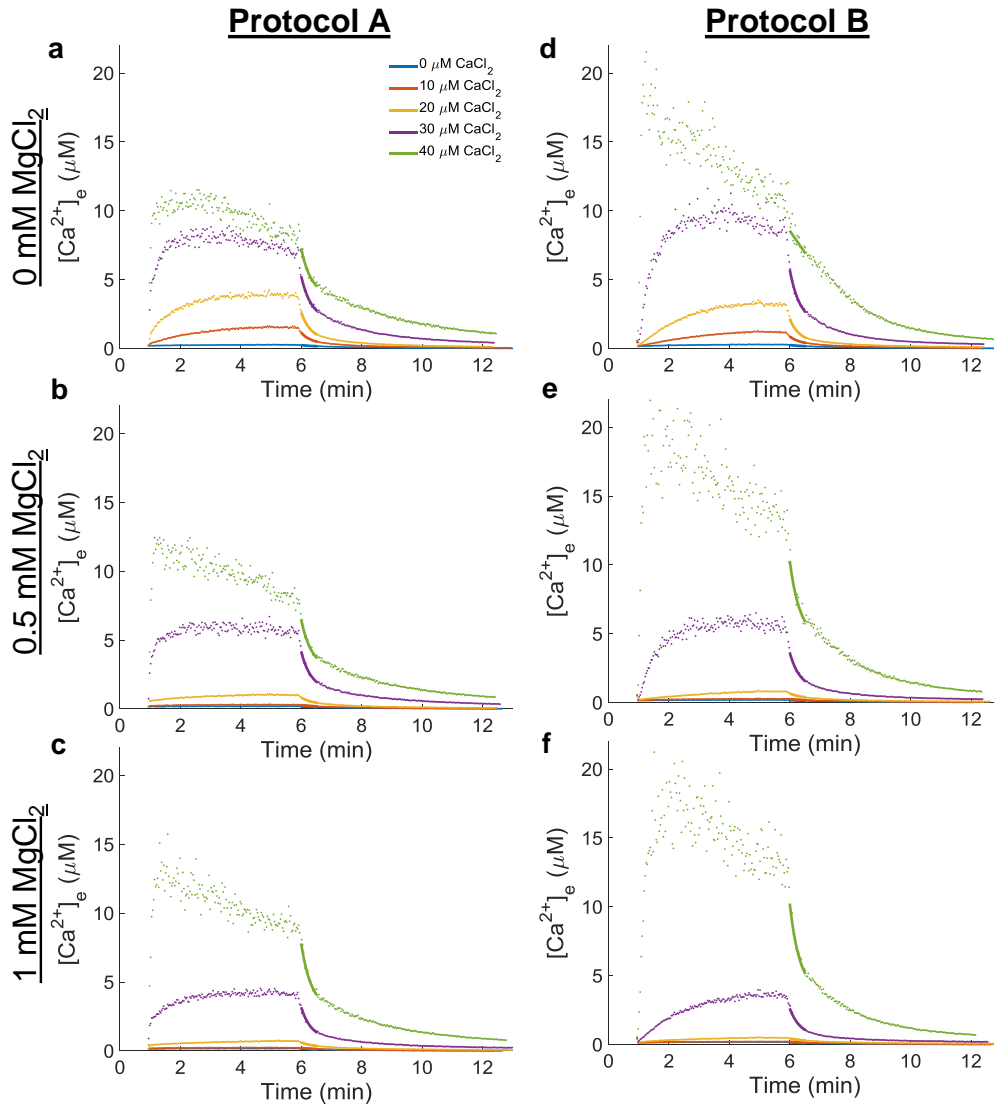


**Fig. S5.** Non-linear trend line fits to the data used to compute matrix Ca<sup>2+</sup> efflux rates. Layout is identical to that shown in Fig. 4 except no error bars are given.

### References:

- Boelens AD, Pradhan RK, Blomeyer CA, Camara KS, Dash RK, Stowe DF (2013) Extra-matrix Mg<sup>2+</sup> limits Ca<sup>2+</sup> uptake and modulates Ca<sup>2+</sup> uptake-independent respiration and redox state in cardiac isolated mitochondria. *J Bioenerg Biomembr* 45(3);203-18.
- Grynkiewicz G, Poenie M, Tsien RY (1985) A new generation of Ca<sup>2+</sup> indicators with greatly improved fluorescence properties. *J Biol Chem* 260(6);3440-3450.
- Molecular Probes. Calcium Calibration Buffer Kits. Revised: 06-July-2001.